

IMPACT OF LOCAL EXTERNAL FORCING OF THE 2006 AUGUSTINE
VOLCANO ERUPTION ON REGIONAL WEATHER CONDITIONS

By

Morgan E. Brown

RECOMMENDED: _____

Advisory Committee Chair

Chair, Department of Atmospheric Sciences

APPROVED: _____

Dean, College of Natural Science and Mathematics

Dean of the Graduate School

Date

IMPACT OF LOCAL EXTERNAL FORCING OF THE 2006 AUGUSTINE
VOLCANO ERUPTION ON REGIONAL WEATHER CONDITIONS

A
THESIS

Presented to the Faculty
of the University of Alaska Fairbanks

in Partial Fulfillment of the Requirements
for the Degree of

MASTER OF SCIENCE

By

Morgan E. Brown, B.S.

Fairbanks, Alaska

August 2008

Abstract

The Augustine Volcano located in South Central Alaska erupted in January 2006 and released water vapor, heat, ash and aerosols into the atmosphere. To determine the impact of these four influences on local weather, 16 simulations are run using the Weather Research and Forecasting (WRF) model. The simulation that excludes any volcano effects serves as a control run and is used to evaluate WRF's performance. Four simulations for each individual factor of heat, water vapor, cloud condensation nuclei (CCN) sized aerosol release and albedo change due to ash fall are run. To analyze interactions, eleven simulations for all possible combinations of factors are also run.

Skill scores and categorical scores are used to quantify the performance of WRF, which indicates that WRF adequately captured the synoptic situation and can be used to evaluate the effect of volcanic eruptions on daily weather.

When considering water vapor, heat, and aerosols, most days experienced statistically significant changes in precipitation and surface temperature. As a result, vertical velocity increased, leading to increased cloud cover and an overall increase in surface temperature. Increasing aerosol particles leads to increased cloud particle numbers with smaller particle diameters, effectively hindering ice particle growth and decreasing precipitation.

TABLE OF CONTENTS

	Page
Signature Page	i
Title Page	ii
Abstract.....	iii
Table of Contents	iv
List of Figures.....	vii
List of Tables	x
Acknowledgments	xi
Chapter 1 Introduction	1
Chapter 2 Experimental Design.....	8
2.1 Model Description	8
2.2 Model Domain.....	15
2.3 Initialization.....	17
2.4 Synoptic Situation	17
2.5 Simulations	19
2.6 Observation Data	24
2.7 Evaluation.....	25
2.7.1 Quantitative Scores.....	25
2.7.2 Categorical Scores	26
2.8 Analysis of Variance	28

Chapter 3 Model Evaluation	34
3.1 General Remarks	34
3.2 Results and Discussion	35
3.2.1 Temperature.....	35
3.2.2 Precipitation.....	42
3.2.3 Sea-level Pressure.....	49
3.2.4 Dew-point Temperature.....	54
3.2.5 Wind Speed	56
3.2.6 Cloud Existence.....	60
3.3 Conclusions from the Evaluation	62
Chapter 4 Augustine Eruption Effects	65
4.1 General Remarks	65
4.1.1 Determining the Error for the ANOVA.....	65
4.2 Results and Discussion	68
4.2.1 Augustine Volcano Effects.....	78
4.2.2 January 25.....	86
4.2.3 February 2.....	91
4.2.4 January 30.....	98
4.2.5 January 29.....	106
4.3 Summary of Augustine Effects	107

Chapter 5 Conclusion.....112

References117

LIST OF FIGURES

Chapter 1

- Figure 1.1 Map of the Cook Inlet region of south central Alaska..... 2
- Figure 1.2 Schematic view of the complexity of volcanic influences on the..... 5

Chapter 2

- Figure 2.1 Schematic of the WRF software components 9
- Figure 2.2 Domain of WRF simulations, centered at the Augustine Volcano 16
- Figure 2.3 Assumed scenario of Augustine’s estimated heat, water vapor, and aerosol release 21
- Figure 2.4 Vector map illustrating ash fall locations extending from the Augustine Volcano..... 23

Chapter 3

- Figure 3.1 Hourly temperature ($^{\circ}\text{C}$) trends as simulated and observed..... 38
- Figure 3.2 Like Fig. 3.1, but for daily maximum temperature ($^{\circ}\text{C}$) 39
- Figure 3.3 Like Fig. 3.1, but for daily minimum temperature ($^{\circ}\text{C}$) 40
- Figure 3.4 Like Fig. 3.1, but for hourly precipitation (mm/h)..... 44
- Figure 3.5 Like Fig. 3.1, but for daily precipitation (mm/d) 45
- Figure 3.6 Hourly observed low-value precipitation events (mm/h) 47
- Figure 3.7 Like Fig. 3.1, but for hourly sea-level pressure (hPa)..... 50

Figure 3.8.1 Hourly pressure (hPa) at the Augustine Volcano observational site	51
Figure 3.8.2 Like Fig. 3.8.1, but for hourly pressure (hPa) at the Palmer observing site.....	52
Figure 3.9 Like Fig. 3.1, but for hourly dew-point temperatures (°C)	55
Figure 3.10 Like Fig. 3.1, but for hourly wind speed (m/s)	57
Figure 3.11 Cloud cover over for Soldotna, Alaska.....	61

Chapter 4

Figure 4.1 Model domain with overlaying domain A, and domain	66
Figure 4.2 Normal Probability plot for January 15, 2006	67
Figure 4.3 Schematic of the microphysical processes that drive changes in precipitation.....	83
Figure 4.4 Schematic representation of the temperature-albedo feedback.....	85
Figure 4.5 Difference between domain B -averaged.....	88
Figure 4.6 Difference in surface	89
Figure 4.7 Vertical cross-section across domain A, diagonally	90
Figure 4.8 Same as 4.6, but for the water vapor and heat release	92
Figure 4.9 Same as 4.6, but for the surface temperature	93
Figure 4.10 Difference between the water vapor release (hVca) and control	96
Figure 4.11 Difference between the water vapor release (hVca) and control	97
Figure 4.12 Same as 4.10 but for the heat and aerosol release.....	99

Figure 4.13 Same as 4.6 but for the heat and aerosol release.....	100
Figure 4.14 Same as 4.10 but for the heat simulation	103
Figure 4.15 Same as 4.6 but for the heat release simulation	104
Figure 4.16 Same as 4.6 but for the heat release simulation	108
Figure 4.17 Same as 4.6 but for cloud ice mixing ratio for heat release	109

LIST OF TABLES

Chapter 2

Table 2.1 Volcanic factors used as treatments for ANOVA significance tests.....	31
---	----

Chapter 3

Table 3.1 Quantitative and categorical skill-scores for WRF simulations.....	36
--	----

Chapter 4

Table 4.1 Bias (treatment minus control) for significant	70
Table 4.2.1 Atmospheric variables with significant volcanic influences.....	72
Table 4.2.2 Same as figure 4.2.1, but for January 11	73
Table 4.2.3 Same as figure 4.2.1, but for January 12	74
Table 4.2.4 Same as figure 4.2.1, but for January 15, 2006.....	75
Table 4.2.5 Same as figure 4.2.1, but for January 17, 2006.....	76
Table 4.2.6 Same as figure 4.2.1, but for January 21, 2006.....	77
Table 4.3 Same as 4.1 but for February 2, 2006.....	79
Table 4.4 Same as 4.1 but for January 30, 2006.....	80
Table 4.5 Same as 4.1 but for January 29, 2006.....	81
Table 4.6 ANOVA summary table.....	87
Table 4.7 Same as 4.5 but for February 2, 2006.....	95
Table 4.8 Same as 4.5 but for January 30, 2006.....	102

ACKNOWLEDGEMENTS

Special thanks to my advisor, Nicole Mölders, for providing the theme for my project, experience, technical help with the code, helpful comments, discussions, guidance. Thanks to my committee, Catherine F. Cahill and Uma S. Bhatt for their comments and helpful discussions; Martha Shulski and NCDC for the observational data; John Dehn for the Augustine heat data; Kristi Wallace for the Augustine ash data; my group members, Debasish PaiMazumder, Zhao Li, Stacy E. Porter, and Theodore Fathauer for their support and guidance; the students and faculty of the Department of Atmospheric Sciences; my family, Ed, Sherry, and Christian Brown for their advice and endless support; and Craig Yarker for his expertise in computer science and endless support.

This project is the result of research supported in part by an International Polar Year student fellowship (Project CIPY-16) through the Cooperative Institute for Arctic Research (CIFAR) with funds from NOAA under cooperative agreement NA17RJ1224 with the University of Alaska; NSF under contracts ATM0232198 and OPP0327664; and Teaching Alaskans...Sharing Knowledge (TASK), a UAF extension of the NSF GK-12 fellowship program.

Computational support was provided by NCAR and in part by a grant of HPC resources from the Arctic Region Supercomputing Center at the University of Alaska Fairbanks as part of the Department of Defense High Performance Computing Modernization Program.

1. Introduction

In January 2006, the Augustine Volcano (located in the Cook Inlet of south central Alaska; 59.4°N; 153.4°W; Fig 1.1) erupted releasing a plume of ash, aerosols, heat, and water vapor into the atmosphere. The explosive phase occurred from January 11 to January 28, then it changed to its continuous phase (steady release of particulates without explosions) until February 2. The largest eruption sequence on January 13 generated a nine-kilometer high plume that extended to the north and northwest (Power et al. 2006). Augustine had a Volcanic Explosivity Index (VEI) of 3 according to the Alaska Volcano Observatory (AVO 2007). The VEI describes strength of a volcanic eruption from the volume of particulates expelled during the eruption on an exponential scale (Newhall and Self 1982). Though the eruption likely was not large enough to affect global climate, the eruption was responsible for ceasing all boat and air traffic for three days in the Cook Inlet, Alaska's largest airport (AVO 2007).

The AVO monitors over 100 active volcanoes in the North Pacific all within close range of populated Alaska regions (Collins et al. 2007). In the past 50 years, 90 Alaska volcanoes have erupted. Thus, it can be anticipated that during the International Polar Year (IPY) active volcanoes will erupt and have an impact on Alaska's economy, local weather and hence may affect ecosystems. Some measurements may be different than they would be without volcanic eruptions.

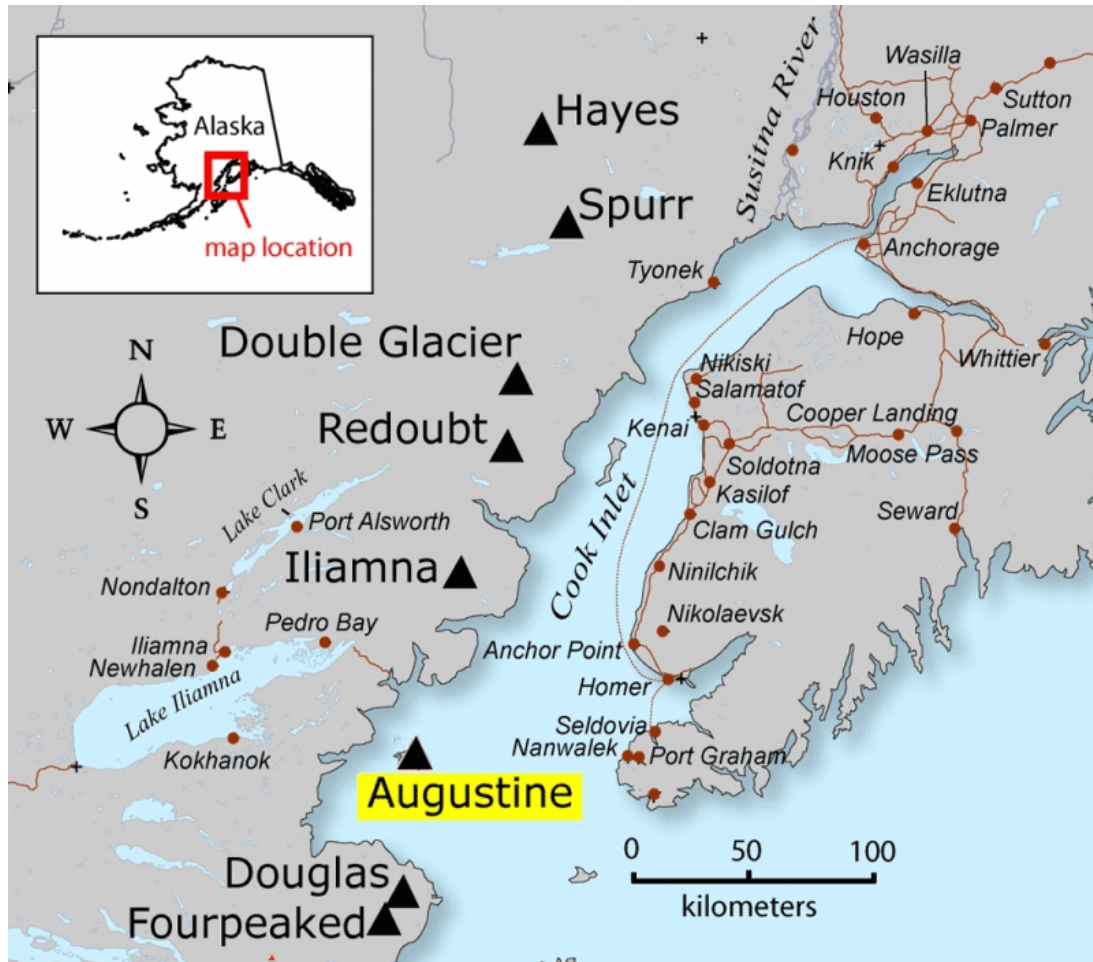


Figure 1.1 Map of the Cook Inlet region of south central Alaska, depicting the location of Augustine Volcano. Map provided by the Alaska Volcano Observatory (AVO 2007).

Volcanic eruptions (regardless of intensity and length) can alter the atmosphere (Robock 2003). General Circulation Models (GCMs) have been used to study the effects of volcanic eruptions on climate. Studies show that large volcanic eruptions can affect both global and regional climate in a variety of ways, like increasing the land-sea temperature gradient (Robock and Mao 1992; 1995) as well as the general circulation in the lower and middle atmosphere (Robock 1996; Kirchner et al. 1999; Robock 2000). It has also been shown that high latitude volcanic eruptions can impact the atmosphere in the lower latitudes (Robock 1981; Robock and Mao 1992; Oman et al. 2005); the release of aerosols into the Arctic stratosphere leads to warming by absorption, which can alter the zonal wind flow (Robock and Mao 1992).

Large volcanic eruptions (such as the 1991 Pinatubo eruption) can alter global and regional temperatures by as much as 4.5K due to the radiative cooling effect of volcanic aerosols in the stratosphere (Wigley et al. 2005). On the local scale, large volcanic eruptions lead to short-term warming, which includes absorption effects from low-level airborne particles and albedo effects due to ash fall (Mass and Robock 1982).

Atmospheric water vapor also plays a role on the impact of large volcanic eruptions. Soden et al. (2002) suggested that more water vapor leads to lower temperatures than we expect from radiative cooling alone.

Aerosols released from volcanic eruptions can lead to stratospheric injection, which leads to radiative cooling for years (Ruddiman 2001). Tropospheric aerosol injection can increase the number of Cloud Condensation Nuclei (CCN) or Ice Nuclei (IN), which provide a surface for water vapor to condense/deposit on to allow for precipitation formation under the right synoptic conditions. Research suggests that such emissions can lead to variations in microphysical processes, which cause changes in atmospheric variables (i.e., temperature and precipitation; Mölders and Olson 2004). The increase of CCN and IN numbers can result into smaller, more numerous cloud droplets as more CCN and IN compete for the excess water vapor, if any. Furthermore, the altered cloud droplet spectrum may yield an increase in cloud cover, but decrease precipitation because smaller droplets hinder the ability for drops to grow to rain-drop-sized diameters (Ruddiman 2001). Figure 1.2 schematically outlines the complex processes associated with volcanic eruptions (Robock 2007).

Volcano effects on the atmosphere start with aerosol release (comprised mostly of sulfur dioxide and dihydrogen sulfur; Fig. 1.2), which absorb and scatter incoming solar radiation, which leads to a net cooling at the surface. Aerosols also scatter longwave radiation, which increases the greenhouse effect of the atmosphere, leading to slight surface warming effects to slightly offset cooling due to a decrease in solar radiation. Aerosols released into the atmosphere include sulfur dioxide particles that undergo chemical reaction in the atmosphere. In the stratosphere, sulfur dioxide depletes ozone, which increases dangerous UV radiation at the surface

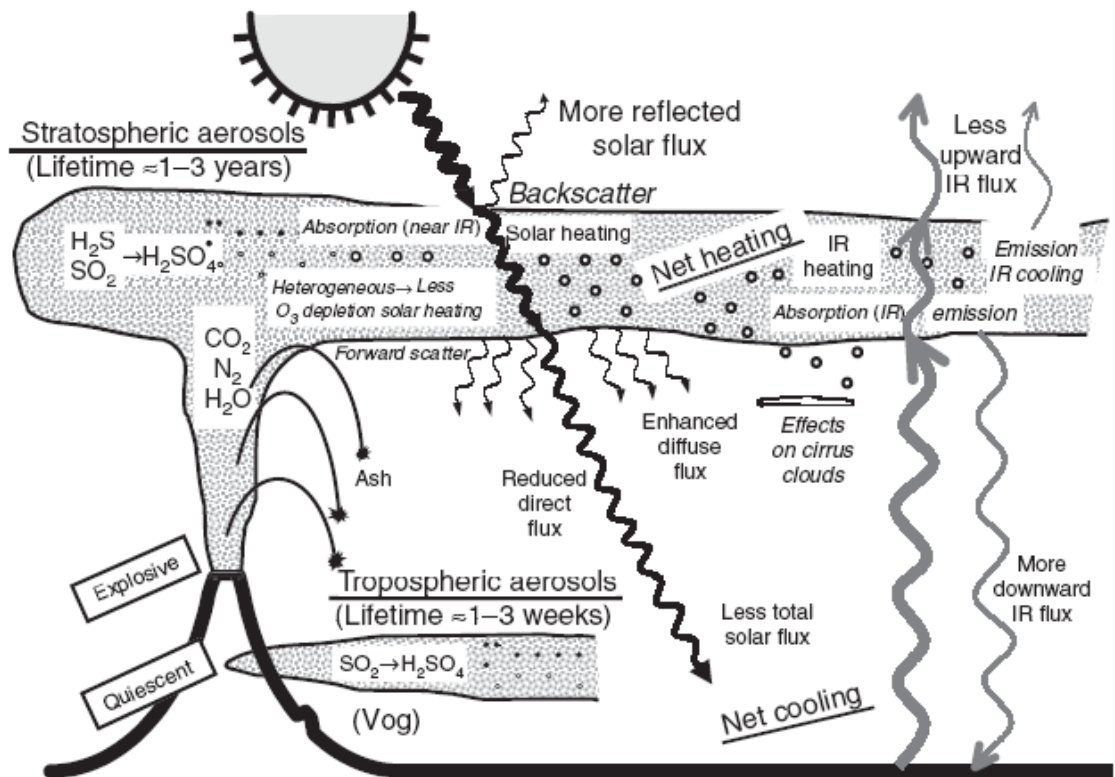


Figure 1.2 Schematic view of the complexity of volcanic influences on the atmosphere (Adapted with permission of Alan Robock, 2003; © American Geophysical Union, 2000).

(Jacob 1999). Lifetime of particles in the stratosphere is on the order of two years for a large eruption, impacting climate globally. Ash fall and aerosol particles that remain in the troposphere absorb solar radiation and increase surface temperature, but these effects are short-lived because tropospheric lifetimes are on the order of two to three weeks (Fig. 1.2). Previous research also suggests that volcanic aerosol release has a stronger impact than anthropogenic aerosol release because volcanic aerosols reach above the turbulent (and rapidly oxidizing) atmospheric boundary layer (Mather et al. 2003).

The majority of studies on the impact of volcanic eruptions on weather and climate were performed for low or mid-latitudes, where large eruptions have economical impact on highly populated areas (e.g. Mass and Robock 1982; Kirchner et al. 1999; Robock 2003; Robock 2007). Given all the potential impacts and complex interactions of processes in response to volcanic eruptions and the unique location of Augustine with respect to the general circulation and climate zone, it is important to investigate whether the small-scale emissions released by the Augustine Volcano could impact local weather. Furthermore, almost all GCMs have shown in greenhouse experiments an amplification of global warming in Polar Regions (e.g., Houghton et al. 1990). Due to various feedback mechanisms, these regions are very sensitive to even slight changes in the water vapor, temperature and altered radiative forcing (e.g., Houghton et al. 1990; Mölders and Olson 2004; Li et al. 2008). Therefore the present study explores the impact of the aforementioned releases on

regional, local (mesoscale γ/β), daily weather. Local weather is on the scale of approximately 20km and 30 minutes according to the scale of mesoscale γ/β . These investigations are based on sixteen simulations performed with the Weather Research and Forecasting (WRF; Skamarock et al. 2005) model.

2. Experimental Design

2.1 Model Description

The Weather and Research Forecasting (WRF; Skamarock et al. 2005) model is a non-hydrostatic (with a hydrostatic option), Eulerian, atmospheric, mesoscale model. This next generation mesoscale and microscale model has been developed by the joint efforts of the scientific community based on experience with previous mesoscale models. In general, WRF simulations begin with input data for initialization that stem from either a global model or reanalysis data. The software framework processes the standard initialization with reanalysis data. It consists of the initialization routine, WRFSI (WRF Standard Initialization), and WRF itself (Fig. 2.1). WRF consists of two dynamics solvers (that can be used alternately) the ARW (Advanced Research WRF) solver (which is primarily developed and maintained by the National Center for Atmospheric Research and described in this study) and the NMM (Non-hydrostatic Mesoscale Model) solver, and a physics package (Skamarock et al. 2005). The WRF is used without consideration of chemical processes.

For the simulations performed in this study, initialization is carried out by using Standard Initialization (SI), where GriB formatted reanalysis data is processed to the real-data ARW system prior to the simulation.

Out of the variety of options the following physics schemes are chosen for the reasons discussed in the following: The Thompson et al. (2004) microphysics

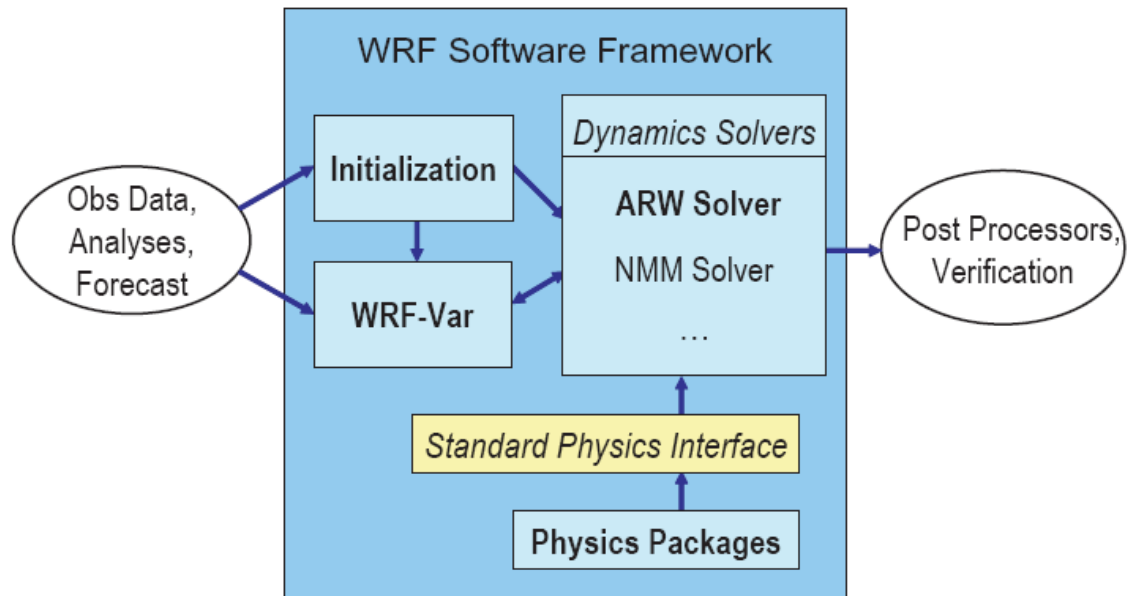


Figure 2.1 Schematic of the WRF software components.

scheme is used. This scheme takes into account seven different moisture variables (cloud-water, rainwater, cloud ice, snow, graupel, number concentration of cloud ice, and number concentration of cloud droplets), including the number of ice particles per grid cell and vertical layer; as well as an ice nucleation parameter, as described in Cooper (1986). This parameterization allows us to add cloud condensation nuclei (CCN) and ice nuclei (IN) from the Augustine Volcano and investigate their impact on cloud and precipitation formation processes and allows for consideration of ice particles, which is important for arctic wintertime conditions. If conditions are favorable for cloud ice or droplet growth (i.e., there is adequate moisture available), cloud droplets will grow on CCN and ice grows on IN in the parameterization scheme. In the Thompson et al. (2004) microphysics scheme, the number of CCN is described using autoconversion formulae (Berry and Reinhardt 1974),

$$\frac{dq_i}{dt} = \frac{2.7 \times 10^{-2} q_c \left[\frac{1}{16} \times 10^{20} D_{\text{mean}}^4 (1 + \nu)^{-0.5} - 0.4 \right]}{\rho_a q_c \left[0.5 \times 10^6 D_{\text{mean}} (1 + \nu)^{-1/6} - 7.5 \right]^{-1}} \quad (2.1)$$

where q_r is the rain water content (g /kg), q_c is the cloud water content (g /kg), $\nu = 3$ is the gamma distribution (continuous probability distribution) shape parameter, ρ_a is the density of air (kg/m^3), and D_{mean} is the mean diameter (m) of cloud droplets given by (Berry and Reinhardt 1974)

$$D_{\text{mean}} = \left(\frac{\Gamma 6 \rho_a q_c}{\pi \rho_w N_c} \right)^{1/3} \quad (2.2)$$

where N_c is the cloud-water droplet number concentration and ρ_w is the density of water (kg/m^3). In the atmosphere, cloud particles can grow in the presence of nucleation particles. Thus, when more CCN and IN are available, water vapor in excess of the saturation water vapor pressure will condense into more cloud particles than it would if only a few CCN or IN were available (Rogers and Yau 1989). Equations 2.1 and 2.2 indicate that more nucleation allows a higher concentration of cloud drops and cloud ice to form; however the particles are smaller because there is more competition between the cloud particles for the available excess vapor. Smaller cloud particle diameters and more competition for available water vapor means droplets are more likely to evaporate once they enter unsaturated regions (Rogers and Yau 1989; Pruppacher and Klett 1997). Moreover, droplet growth by collection is reduced, which effectively hinders rainwater formation (Eqn. 2.1). Thus, precipitation will likely decrease, if the amount of IN and CCN increase.

Cumulus convection is of sub-grid scale for the resolution used in this study, so the Grell-Devenyi cumulus scheme (Grell-Devenyi 2002) is used to consider the effects of subgrid-scale convection. This scheme is a mass-flux, ensemble cumulus scheme. This cumulus scheme effectively runs multiple cumulus schemes within each grid box and averages their results (using equal weight averaging), then provides the feedback to WRF. The scheme assumes different updraft and downdraft entrainment and detrainment parameters and the dynamic controls are

described by convective available potential energy (CAPE), low-level vertical velocity, and moisture convergence.

The Rapid Update Cycle (RUC) land-surface model (LSM; Smirnova et al. 1997; 2000) is used because of its multiple layer snow model, consideration of frozen soil physics, and the vegetation canopy variations. Frozen soil physics is important for simulations in Alaska because there is considerable extent of permafrost, which can impact the moisture exchange between the soil and atmosphere (Mölders et al. 2003; Mölders and Walsh 2004). Multiple snow layers allow for more accurate calculation of the radiation budget, as well as better prediction of soil temperatures and surface fluxes (Fröhlich and Mölders 2002). Multiple snow layers capture changes in mesoscale variables (such as near-surface air temperatures and humidity, latent heat fluxes, and soil heat fluxes) better than varying emissivity and albedo (Fröhlich and Mölders 2002). The RUC LSM considers varying snow depth per grid cell as well as snow temperature and density variations. For albedo considerations, this scheme considers snow-albedo as a function of snow depth and time since last snowfall.

In this scheme, each new snow event refreshes snow albedo values. Thus, the formulation of the scheme easily allows for introducing volcanic ash fall by albedo readjustment if ash-fall occurs during the simulation.

The RUC surface balance equations (Smirnova et al. 2000) are the key processes that consider heat and atmospheric water vapor. The difference between

the water vapor at the surface and in the near-surface atmosphere is important in determining evaporation (Smirnova et al. 1997)

$$E = -\rho_a K_q \left. \frac{\partial q_v}{\partial z} \right|_{\Delta z_a} \quad (2.3)$$

where E is the evaporation, ρ_a is the air density at the surface (kg/m^3), K_q is the turbulent moisture exchange coefficient (m^2/s), and z is the vertical coordinate (terrain following σ coordinate). Evaporation is then used in the soil moisture balance equation (Smirnova et al. 1997)

$$\rho_w \frac{\partial \eta_g}{\partial t} = \frac{\partial}{\partial z} (W_s + I - E) \quad (2.4)$$

where ρ_w is the density of water (kg/m^3), η_g is the volumetric water content at the soil surface (unit-less ratio of water volume to soil volume), W_s is the moisture flux into the ground ($\text{kg/m}^2\text{s}$), I is the infiltration flux ($\text{kg/m}^2\text{s}$), and E is atmospheric evaporation in the lowest vertical layer ($\text{kg/m}^2\text{s}$).

The change in surface temperature is determined by means of the heat budget equation for bare soil (Smirnova et al. 1997)

$$\rho_s c_s \frac{\partial T_g}{\partial t} = \frac{\partial}{\partial z} (R_n - H - L_v E + G) \quad (2.5)$$

and for vegetated surfaces (Smirnova et al. 1997)

$$\left(\rho_a c_p \Delta z_a + \rho_s c_s \Delta z_s \right) \frac{\partial T_g}{\partial t} = \left(R_n - H - L_v \left\{ E_{\text{dir}} (1 - \sigma_f) + E_c \sigma_f + E_t \sigma_f \right\} \right) \Big|_{\Delta z_a} - G \Big|_{\Delta z_s} \quad (2.6)$$

where T_g is the temperature at the ground surface, R_n is the net radiation into the layer as a function of albedo (which is snow covered for the domain considered in this study), H is the sensible heat flux, $L_v E$ is the latent heat flux, G is the ground heat flux, ρ_s is the soil density, c_p and c_s are the specific heat of air under constant pressure and the specific heat of soil, respectively, E_{dir} is the evaporation flux from bare soil, L_v is the latent heat of vaporization, σ_f is the shielding factor (this scheme sets it to 0.7), E_c is the evaporation of water intercepted by the canopy, and E_t is the transpiration. For snow cover, equation 2.6 replaces ρ_s , c_s , and Δz_s with the snow cover equivalents ρ_{sn} , c_{sn} , and Δz_{sn} . In chapter 2.5, a detailed description of how the volcanic heat and water vapor fluxes are implemented into the WRF model using these equations is described.

Furthermore, the Yonsei University (YSU; Hong and Pan 1996) atmospheric boundary layer scheme is applied, which assumes non-local gradient fluxes. It also considers entrainment at the top of the atmospheric boundary layer (ABL). This scheme is the next generation Medium Range Forecast Model (MRF) scheme, which considers the ABL height from the buoyancy profile.

Finally, the Rapid Radiative Transfer Model (RRTM; Mlawer et al. 1997) and the Dudhia (1989) scheme are used for treating long-wave and shortwave radiation, respectively. The long-wave radiation scheme considers multiple bands, trace gases, and microphysical species (i.e., cloud and precipitation particles) in determining long-wave radiation. Thus, it permits us to investigate feedback

processes between liquid and solid cloud particles and radiation. At the lower boundary, the scheme is coupled with the LSM by variables, such as latent heat flux and sensible heat. The short-wave radiation-scheme takes into account cloud optical depth, cloud albedo, clear-sky absorption and scattering. The shortwave radiation scheme is coupled with the LSM via albedo, and net radiation is coupled with the longwave radiation scheme. Both the RRTM and Dudhia schemes have already been used in the fifth-generation Pennsylvania State University-National Center for Atmospheric Research Mesoscale Meteorological Model (MM5; Grell et al. 1995), which is an older mesoscale model that has been evaluated extensively, even in sub-arctic conditions (Mölders and Olson 2004; Narapusetty and Mölders 2005).

2.2 Model Domain

The domain (Fig. 2.2) is centered over the Augustine Volcano on Augustine Island, Alaska (59.4°N; 153.4°W). The island that is made up entirely of volcanic deposits extends 8 km by 11 km, and is located in South Central Alaska about 275 km southwest of Anchorage (AVO 2007). Terrain is dominated by an inlet, costal region surrounded by the Pacific Mountain System. WRF is run using a four-kilometer grid increment with 149x149 grid points in the horizontal directions and 31 vertical layers. This horizontal grid requires the use of the non-hydrostatic option for the simulations because the hydrostatic approximation is only valid on large

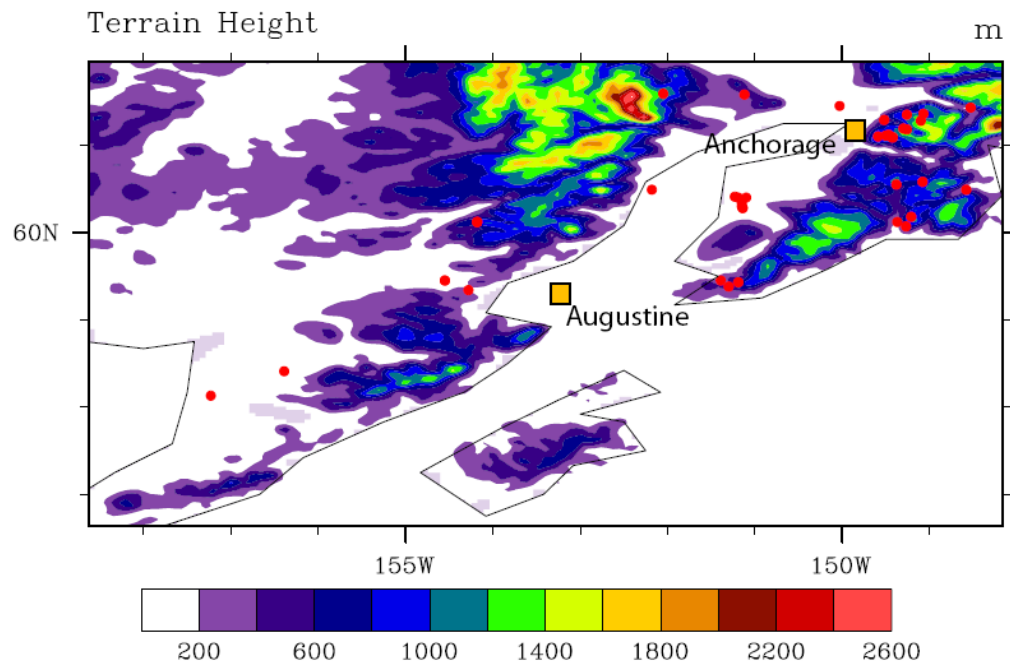


Figure 2.2 Domain of WRF simulations, centered at the Augustine Volcano at 59.4°N and 153.4°W with 149×149 grid points at 4km resolution. Terrain height is contoured in meters and the black markers indicate observation station locations.

horizontal (climate) scales. A time step of 24 seconds is used, which is the WRF ARW recommended time step for the grid size used in this study.

2.3 Initialization

Initial and boundary conditions are from $1.0^{\circ} \times 1.0^{\circ}$, six-hour, global final analysis (FNL) National Center for Atmospheric Research (NCAR) and National Centers for Environmental Protection (NCEP) reanalysis data. WRF is run once a day (i.e., restarted once every 24 hours) for a period of 25 days, from January 10 through February 2, 2006. Land-use and soil data is from the US Geological Survey (USGS). Snow cover and sea ice is initialized from the reanalysis data.

2.4 Synoptic Situation

The period of this study began on January 10, 2006 with a weakening low-pressure system over the Gulf of Alaska, which eventually shifted to a weak high over the Alaska Inlet peaking on January 13. A weak low caused slight drops in pressure on January 17, with precipitation over the area through January 18. On January 21, a strong pressure system developed over the Aleutian Islands, causing a significant pressure drop over the next two days. Moving northward, it brought heavy precipitation (as much as twenty millimeters) and strong winds to the area. By January 24, sea-level pressure increased back to normal levels. On January 25, a weaker low began to move northward, dropping pressure and causing some slight

precipitation for parts of the region at the end of the period (January 25 through February 2).

At the beginning of January 2006, temperatures were unusually high (approximately 8K above climate normal) because the region was experiencing southerly flow under a ridge in the synoptic wave pattern. On January 21, when the major cyclone came through, there was a drop in temperatures across the region, bringing values back to seasonably normal (approximately -12°C ; Shulski and Wendler 2007). At the beginning of the month, maximum temperatures ranged from -12°C to 4°C ; at the end of the month, maximum values ranged from -23°C to -6°C .

Wind speeds during January 2006 usually stayed below 5m/s in most locations; though during the mid-month cyclone, some areas recorded winds speeds as high as 20m/s. Other areas maintained accelerated wind speeds of about 10m/s. Average wind speeds for the domain for the month of January are approximately 3m/s (Shulski and Wendler 2007). The prevailing wind direction was from the southwest to southeast in the domain. This means that land and highly populated areas were downwind of the Augustine volcano.

Upper level winds tend to be prevailing westerlies. Therefore, if Augustine erupts high enough, the plume may travel away from the mainland.

2.5 Simulations

Four separate volcanic influences (hereby referred to as factors) are considered in this study. Each of the factors is added to the WRF model by modifying appropriate variables in the WRF code. All scenarios are hypothetical and do not necessarily replicate what actually occurred during the 2006 Augustine eruption. This study is only designed to test the feasibility of a volcanic eruption having an impact on local weather.

Volcanic heat release is introduced into WRF via interpolated temperature values estimated from the NOAA Advanced High Resolution Radiometer (AVHRR; data provided by Dehn, Alaska Volcano Observatory, 2006). Surface temperature in the heat balance equation is replaced with the satellite data (see Eqns. 2.5 and 2.6), which WRF transports vertically during the simulation. This procedure is carried out only for the grid representing Augustine.

The addition of aerosols is established using a simulated dataset of the number of effective CCN released from the volcano in January 2006. The amount of CCN released from the 2006 Augustine eruption is estimated using the criteria for the Volcanic Explosivity Index (Newhall and Self 1982) and a comparison of CCN fluxes measured from previous Alaska volcanic eruptions (e.g., Hobbs et al. 1982; Mather et al. 2003). The amount of CCN release is determined to be between 10^{15} - 10^{17} CCN/s. Aerosol chemistry is not considered in the WRF model, so changes in number of CCN due to chemical reactions do not occur in this study. The range of

CCN release is correlated with the heat input data, such that as the air temperature increases the number of aerosols released also increases (Fig. 2.3). Since previous research has suggested that volcanic aerosol release has a significant impact on climate and regional weather because they reach above the turbulent (and rapidly oxidizing) atmospheric boundary layer (Mather et al. 2003), we include the volcanic aerosol release for the volcano grid cell in WRF. The height of the ABL is generally less than 1 km above the surface for a high-latitude, wintertime scenario (Wallace and Hobbs 2006). The number of CCN in the cloud microphysics scheme is altered to include this increase in aerosol content (please refer to Eqns. 2.1 and 2.2).

Moisture release from the Augustine volcano is simulated using minimum and maximum values measured from previous Alaska volcanic eruptions. Moisture release depends more heavily on the eruption type, as opposed to the size of the eruption like aerosol release (Stith et al. 1978). The Alaska Volcano Observatory descriptions of the 1976 and 2006 eruptions of Augustine have suggested that these eruption patterns were very similar. Since water vapor measurements were carried out for the 1976 eruption (Stith et al. 1978; Hobbs et al. 1991), the range of these values is assumed to be the valid also for the 2006 eruption. For simplicity, water vapor values are correlated with the observed heat release (as for the aerosol release), with values ranging from 1×10^2 kg/s (during the effusive, non-explosive phase) to 1×10^5 kg/s (during the explosive phase). In the grid-cell wherein Augustine is located, the water vapor mixing ratio is enhanced according to the described release

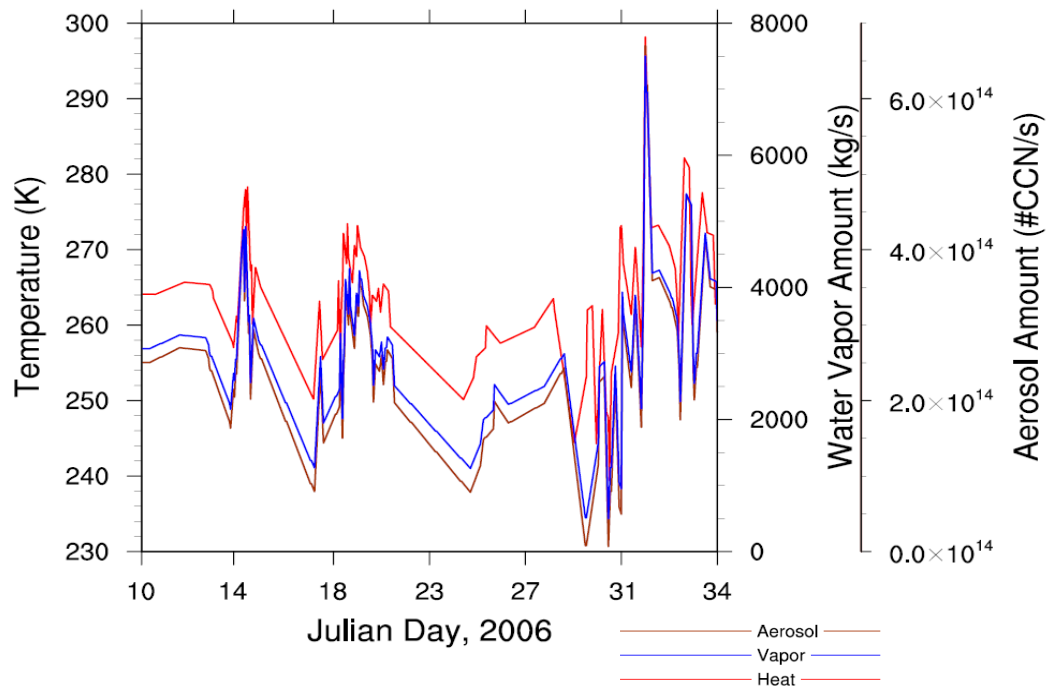


Figure 2.3 Assumed scenario of Augustine’s estimated heat, water vapor, and aerosol release. Temperature measurements (volcanic heat) are estimated from the AVHRR (provided by Dehn, 2006). Water vapor and aerosol data are correlated with the heat trends based on maximum and minimum values obtained from previous high-latitude volcanic eruption observed data. See section 2.5 for details and explanations. The brown, blue, and red lines refer to the aerosol number increase, water vapor increase, and surface temperature increase, respectively, that are used in the simulations where aerosols, water vapor, and heat release are considered.

scenario in the first layer above ground to include the addition of the volcanic water vapor (see Eqns. 2.3 and 2.4).

Figure 2.3 shows the trends for aerosol and vapor release correlated with the heat release data from AVO. Scenarios for heat, water vapor, and aerosol release are interpolated across the 24-day period as a continuous, variable volcanic eruption, which is not necessarily what occurred during the actual Augustine eruption.

Volcanic ash fall locations are obtained from the Alaska Volcano Observatory (provided by Wallace, Alaska Volcano Observatory, 2006). Vector maps showing the projection of ash fall per day are used to determine albedo changes (Fig. 2.4). Using the trajectories available, ash fall projections are assumed to be at a 45° dispersion angle from the Augustine grid cell, centered at the corresponding vector for each day. Since amount of ash deposited per trajectory is not available at the time of the simulations, albedo changes based on the amount of ash fall is not considered. Thus, it is assumed that for all grid cells within the ash fall projection angle, albedo decreases by 10% of its original value at the beginning of each simulation. Albedo changes are considered in the LSM model within the equation that determines albedo based on snow depth, so that any snowfall during the day would increase the albedo correspondingly.

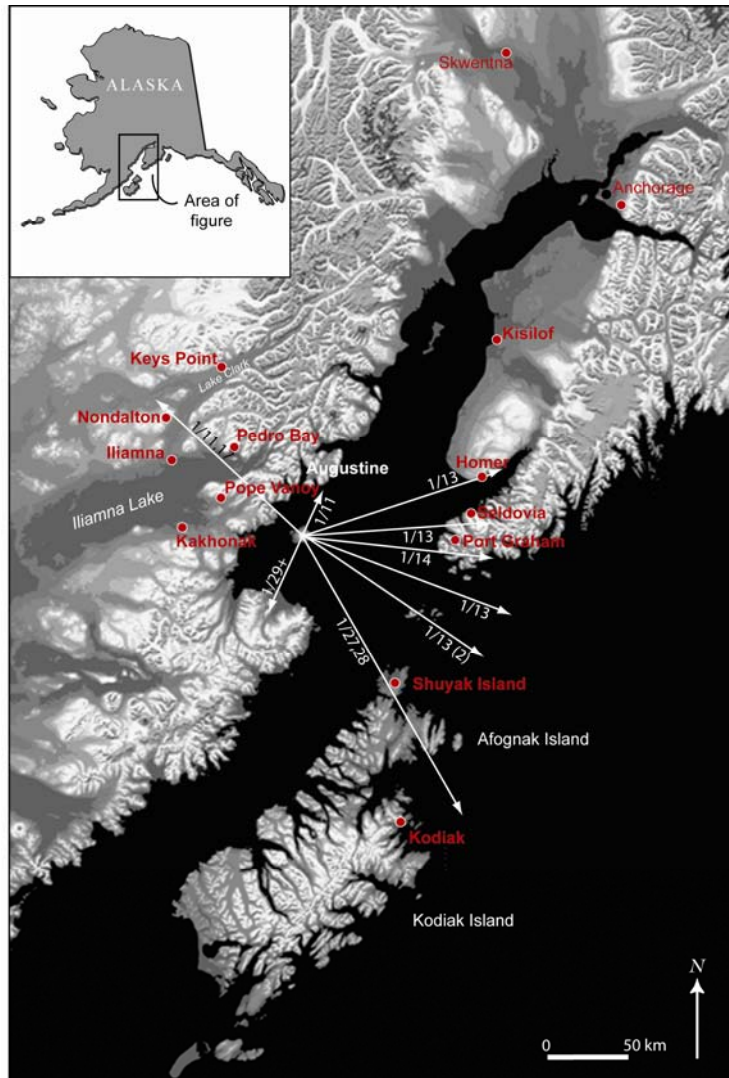


Figure 2.4 Vector map illustrating ash fall locations extending from the Augustine Volcano. WRF simulated ash fall projections are assumed to be at a 45° dispersion angle from the Augustine grid cell, centered at the corresponding vector for each day. Image provided by Wallace (2006, Alaska Volcano Observatory).

2.6 Observation Data

To evaluate WRF's performance, simulated data is compared with data from 43 observing sites within the Cook Inlet region. Figure 2.2 shows the model domain. Observational data is provided by the National Climatic Data Center (NCDC) via the Alaska Climate Research Center (ACRC). Atmospheric variables evaluated include 17 stations with hourly data (cloud cover, wind speed, pressure, temperature, dew point, precipitation) and 26 stations with daily data (precipitation, maximum temperature, minimum temperature). Observing sites are considered representative of their respective WRF grid cell for evaluation purposes. This procedure is common in mesoscale modeling (e.g., Anthes 1983; Anthes et al. 1989; von Storch and Zwiers 1999; Narapusetty and Mölders 2005; Zhong et al. 2005; PaiMazumder et al. 2007).

Since WRF does not determine cloud cover fraction, cloud existence is used instead. This quantity is determined as follows: if WRF simulates a mixing ratio greater than 0.001 kg/kg for any vertical layer in a grid cell, it will be assumed that clouds exist in the volume represented by the grid-cell. Correspondingly, if an observing site reports any fraction of the sky as cloud covered, a cloud will exist. This procedure for cloud evaluation is common practice in model evaluation (e.g., Anthes et al. 1989; PaiMazumder et al. 2007).

2.7 Evaluation

For objective analysis, quantitative and categorical skill scores are calculated (e.g., Anthes 1983; Anthes et al. 1989; von Storch and Zwiers 1999; Narapusetty and Mölders 2005; Zhong et al. 2005). Quantitative skill scores evaluate how close a point simulation (or forecast) value is from the true value (i.e., observed value). Categorical skill scores assess a forecast under consideration of events, rather than point forecasts. Evaluation using categorical skill scores considers how frequently an event occurred compared to the number of times the event is forecasted.

2.7.1 Quantitative Scores

The bias indicates systematic errors

$$\bar{\phi} = \frac{1}{n} \sum_{i=1}^n \phi_i \quad (2.7)$$

which occur from errors due to parameterizations, assumptions on model parameters, misinterpretation of the landscape (terrain height, land-cover type, soil type, etc.), discretization or other numerical errors. Here, ϕ_i is the difference between the simulated and observed quantity to be evaluated at a given grid point, i , in time. n represents the total number of data points summed. The standard deviation of error

$$\text{SDE} = \left(\frac{1}{n-1} \sum_{i=1}^n (\phi_i - \bar{\phi})^2 \right)^{1/2}. \quad (2.8)$$

represents random errors related to initialization and boundary conditions and/or measurement errors. To evaluate the overall performance, the root-mean-square error

$$\text{RMSE} = \left(\frac{1}{n-1} \sum_{i=1}^n (\phi_i)^2 \right)^{1/2} \quad (2.9)$$

is calculated.

2.7.2 Categorical Scores

To determine the performance for categorical atmospheric variables, such as precipitation and cloud presence, threat score, accuracy, probability of detection, and the Heidke score are used (Anthes et al. 1989; von Storch and Zwiers 1999; Zhong et al. 2005). These equations are evaluated based on the following contingency tables: N_1 when an event is simulated and observed, N_2 when an event is simulated but not observed, N_3 when an event is observed but not forecasted, and N_4 when an event is not simulated and not observed.

The threat score is then defined as

$$\text{TS} = \frac{N_1 + N_4}{N_1 + N_2 + N_3} \quad (2.10)$$

which is an evaluation of the number of correct simulations to the total events either simulated or observed. The threat-score indicates the success in correctly forecasting an event at a site. It is sensitive to hits and punishes false alarms and misses. In general, larger threat score values indicate a better simulation. A threat score of 1

does not indicate a perfect simulation because if $TS=1$, the numerator and denominator of Eqn 2.10 must be equal. For this to be the case, either N_2 or N_3 must be greater than zero, indicating the simulation incorrectly forecasted a number of events.

The accuracy is defined as:

$$\text{Accuracy} = \frac{N_1 + N_4}{N_1 + N_2 + N_3 + N_4} \quad (2.11)$$

which is sensitive to the number of correctly simulated events compared to all events. Accuracy gives the fraction of correct predictions. A perfect accuracy score is 1, whereas a perfect threat score is subjectively based on the number of events. Accuracy can be misleading because it is heavily influenced by the most common category. For example, events that rarely occur during a period of interest are generally dominated by the N_4 scenario (e.g., high fire-risk, heavy precipitation).

To compare the categorical scores to random chance, the Probability of Detection and the Heidke skill score (von Storch and Zwiers 1999) are determined. Both of these scores calculated the occurrence over a threshold. Generally, a threshold value of 0.25 mm per time (either per hour or day, depending on the observation data set) is used for evaluating a precipitation forecast (Anthes 1983), which also roughly coincides with the average precipitation per event for South Central Alaska (the Cook Inlet region) in January (Shulski and Wendler 2007). Thus, a threshold value of 0.25 mm/h will be used for determining the Probability of Detection and the Heidke skill score.

The Probability of Detection (or categorical score) uses the same contingency table described above and can be defined as:

$$\text{PoD} = \frac{N_1}{N_1 + N_3} . \quad (2.12)$$

This score only considers the number of simulated events, so a perfect Probability of Detection score would be 1 (i.e., all events simulated above the given threshold were observed).

In accordance with Wilks (1995) and Zhong and Fast (2003), the Heidke skill score is defined as:

$$\text{HSS} = \frac{2(N_1N_4 - N_2N_3)}{(N_1 + N_3)(N_3 + N_4) + (N_1 + N_2)(N_2 + N_4)} \quad (2.13)$$

such that a perfect forecast yields $N_2 = N_3 = 0$, thus $\text{HSS} = 1$. When $N_1N_4 = N_2N_3$, $\text{HSS} = 0$ and the forecast skill is based on random chance. If HSS is negative, forecast skill will be worse than random chance.

2.8 Analysis of Variance

Four separate volcanic factors and all combination of them are considered in this study: release of heat, aerosols and water vapor as well as albedo change due to ash-fall. To analyze interactions, a total of sixteen WRF simulations are performed; one control run (no volcanic factors, simulation hvca), four for each individual factor (hvca, hVca, hvCa, hvcA), and eleven for all possible combinations of factors. Here the letters H, V, C, and A stand for the release of heat, water vapor, and aerosols and

ash-fall, respectively. Capital letters represent the factor switched on, small letter denote to the factor switched off.

To determine which factor or combination of factors, (hereby referred to as treatments) have a significant impact on the weather, Analysis of Variance (ANOVA) is used (e.g., Montgomery 1976). Recently, various studies have been applied to analyze factor interaction in climate and meteorological research (e.g. Mölders and Olson 2004; Caires et al. 2006; Li et al. 2008).

In this study, a 2^4 -factorial design is used that assumes (1) fixed factors, (2) a randomized design, and (3) that each treatment satisfies the assumption of normality (Montgomery 1976). The exponent represents the number of factors this study considers (4: heat, vapor, aerosols, and ash) and the base represents the level (in this case, 2, either off or on).

The ANOVA design begins with a null hypothesis, where significance is tested using an f-test. ANOVA generates f-values for all treatments, which are compared to expected test statistic values at the 95% confidence level. If ANOVA f-test values are larger than the expected values, the null hypothesis will be rejected. For this study, the **null hypothesis** is that *there is no significant change in the weather from volcanic influence*.

To perform the f-test, the Sum of Squares is calculated for all treatments. As described by Montgomery (1976), the sum of squares can be determined by

$$SS_{ijkl} = \frac{1}{n 2^4} (\text{Contrast}_{ijkl})^2 \quad (2.14)$$

where n is the number of replicates (i.e., the number of values for each treatment over space and time) and i , j , k , and l represent the two levels (on or off) of the volcanic factors heat, water vapor, aerosol, and ash fall, respectively. Contrast is defined as

$$\text{Contrast}_{ijkl} = (i + 1)(j + 1)(k + 1)(l + 1) \quad (2.15)$$

where treatments that are turned off are subtracted by 1 (here, the 1 represents the control run) and factors turned on are added to 1. For example, the contrast for the heat simulation (heat is turned on and the other three factors are turned off) can be written as

$$\text{Contrast}_i = (i + 1)(j - 1)(k - 1)(l - 1) \quad (2.16)$$

For this study, each variable (e.g., precipitation, water vapor mixing ratio, temperature) is summed across the domain of interest and time such that there is only one replicate; hence, there is only one value per treatment, per variable, per day. This procedure is typically adopted for higher order ANOVA designs, since the number of treatments to consider is very large (e.g., Montgomery 1976). Table 2.1 illustrates the treatments used in this study.

When determining the contrast of a treatment, i , j , k , and l represent the treatment (not the value) and the 1 represents the control (i.e., all volcanic factors are turned off). For example, the tertiary interaction treatment is defined as

Table 2.1 Volcanic factors used as treatments for ANOVA significance tests. Atmospheric variables (e.g., precipitation and temperature) are tested by summing across the domain of interest and time such that there is only one replicate per day. H, V, C, and A represent volcanic factors heat, water vapor, aerosols, and ash turned on, respectively. Lower case h, v, c, and a represent heat, water vapor, aerosols, and ash turned off, respectively.

Heat on					
		Vapor on		Vapor off	
		Ash on	Ash off	Ash on	Ash off
Aerosol on	$\sum X_{HVCA}$	$\sum X_{HVCa}$	$\sum X_{HvCA}$	$\sum X_{HvCa}$	
Aerosol off	$\sum X_{HvCa}$	$\sum X_{HVCa}$	$\sum X_{HvcA}$	$\sum X_{Hvca}$	

Heat off					
		Vapor on		Vapor off	
		Ash on	Ash off	Ash on	Ash off
Aerosol on	$\sum X_{hVCA}$	$\sum X_{hVCa}$	$\sum X_{hvCA}$	$\sum X_{hvCa}$	
Aerosol off	$\sum X_{hVca}$	$\sum X_{hVCa}$	$\sum X_{hvcA}$	$\sum X_{hvca}$	

$$\text{Contrast}_{\text{HVCA}} = (H - 1)(V - 1)(C - 1)(A - 1) \quad (2.17)$$

which can be expanded to

$$\begin{aligned} \text{Contrast}_{\text{HVCA}} = & \text{HVCA} - \text{HVCa} - \text{HVcA} - \text{HvCA} - \text{hVCA} \\ & + \text{hvCA} + \text{hVcA} + \text{HvcA} + \text{hVCa} + \text{HvCa} + \text{HVca} - \text{Hvca} \\ & - \text{hVca} - \text{hvCa} - \text{hvcA} + 1 \end{aligned} \quad (2.18)$$

where the interaction treatments are represented by combined individual factors (e.g., HVCa and hVcA).

Atmospheric variables can be broken down into individual effects, interaction effects, and error effects. Hence, the ANOVA linear model (in terms of the sum of squares) is defined as the total sum of squares for all factors.

$$SS_T = SS_E + \sum_i \sum_j \sum_k \sum_l SS_{ijkl} \quad (2.19)$$

where SS_E is the error. For unreplicated ANOVA designs, SS_E is determined by plotting treatment estimates against their probability (for example, refer to Fig. 4.2). Non-significant treatments have a linear fit and, thus, can be assumed as error (Montgomery 1976).

To test the hypothesis, the sum of squares value is divided by the degrees of freedom to get the mean square (MS). If the null hypothesis is true, it can be expected that

$$MS_{ijkl} = \sigma^2 \quad (2.20)$$

where MS_{ijkl} represents the treatments analyzed and σ^2 is the standard deviation. If they are not equal, determining the f-value will test significance

$$f_{\text{calc}} = \frac{MS_{ijkl}}{MS_E}, \quad (2.21)$$

where if F_{calc} is greater than F_{table} (the expected f-test value), we can reject the null hypothesis concluding that the respective volcanic treatment has a significant impact on the weather.

3. Model Evaluation

3.1 General Remarks

WRF is a new generation mesoscale model; many of its parameterizations are recoded from its well-evaluated predecessor, the Pennsylvania State University-National Center for Atmospheric Research Fifth-Generation Mesoscale Model (MM5; Grell et al. 1995). WRF has been evaluated extensively since its release mainly for the contiguous US states (e.g., Skamarock 2004; Otkin and Greenwald 2008). Some efforts have been made to evaluate WRF for Arctic regions (Henderson et al. 2007; Mölders 2008). It is important to evaluate models because error propagation due to initialization, boundary conditions, parameterizations, and/or grid resolution can impact predicted atmospheric variables (e.g., Pielke 2002; Anthes et al. 1989; Narapusetty and Mölders 2005; PaiMazumder et al. 2007).

A common source of error, as discussed in previous evaluation studies, is the discrepancy between grid cell volumetric quantities in simulated data vs. point measurements as taken from observation data (e.g., Avissar and Pielke 1989; Seth et al. 1994; Boone et al. 2004; Zhong et al. 2005). In mesoscale modeling evaluation studies, it is commonly assumed that observation sites are representative of their respective grid cell (e.g., Anthes et al. 1989; Narapusetty and Mölders 2005; Zhong et al. 2005). Error as a consequence of this assumption is well known and has been discussed widely (e.g., Anthes et al. 1989; Avissar and Pielke 2002; Seth et al. 1994; Boone et al. 2004; Zhong et al. 2005).

3.2 Results and Discussion

In general, WRF tends to overestimate precipitation, temperature, wind speed, and dew-point temperatures for the episode examined in this study. Conversely, pressure and cloud existence are generally underestimated. Table 3.1 summarizes the skill-scores for the WRF simulations, where the bias indicates if the variable is underestimated (negative bias) or overestimated (positive bias).

3.2.1 Temperature

Over the study period, WRF and observational variations generally follow each other for hourly and daily temperature values (Figs. 3.1, 3.2 and 3.3), but WRF almost always overestimates temperature. Table 3.1 indicates that skill-scores are lower for daily maximum temperature than daily minimum temperature, which suggests that WRF-predicted diurnal cycles are slightly dampened compared to observations.

Overall, daily temperature RMSE, SDE, and bias (4.5 K, 3.8 K, and 1.2 K, respectively) are comparable to those found for other synoptic situations by Nutter and Manobianco (1999) and Zhong et al. (2005). RMSE and SDEs of hourly temperatures are about 1 K to 2 K lower than those from Nutter and Manobianco (1999) and Zhong et al. (2005). This means that obviously WRF's performance is reliable despite potential impact of the volcanic eruption and is slightly better than

Table 3.1 Quantitative and categorical skill-scores for WRF simulations: bias, standard deviation of error (SDE), root mean square error (RMSE), threat score, accuracy, Heidke skill score (HSS), probability of detection (PoD).

	Hourly						
	Bias	SDE	RMSE	Threat Score	Accuracy	HSS	PoD
Temperature (K)	0.0	0.7	0.7	---	---	---	---
Precipitation (mm/h)	-0.0	0.0	0.0	0.1	0.9	0.1	0.4
Pressure (hPa)	-0.0	0.4	0.4	---	---	---	---
Dew-point (K)	0.1	0.7	0.7	---	---	---	---
Wind Speed (m/s)	0.0	0.4	0.5	---	---	---	---
Cloud Existence	-0.1	0.4	0.8	0.4	0.6	0.1	0.3

Table 3.1 continued

	Daily						
	Bias	SDE	RMSE	Threat Score	Accuracy	HSS	PoD
Max. Temperature (K)	0.1	3.5	4.0	---	---	---	---
Min. Temperature (K)	2.1	4.8	5.5	---	---	---	---
Avg. Temperature (K)	1.2	3.8	4.5	---	---	---	---
Precipitation (mm/d)	1.0	1.5	2.4	0.1	0.9	0.5	0.9

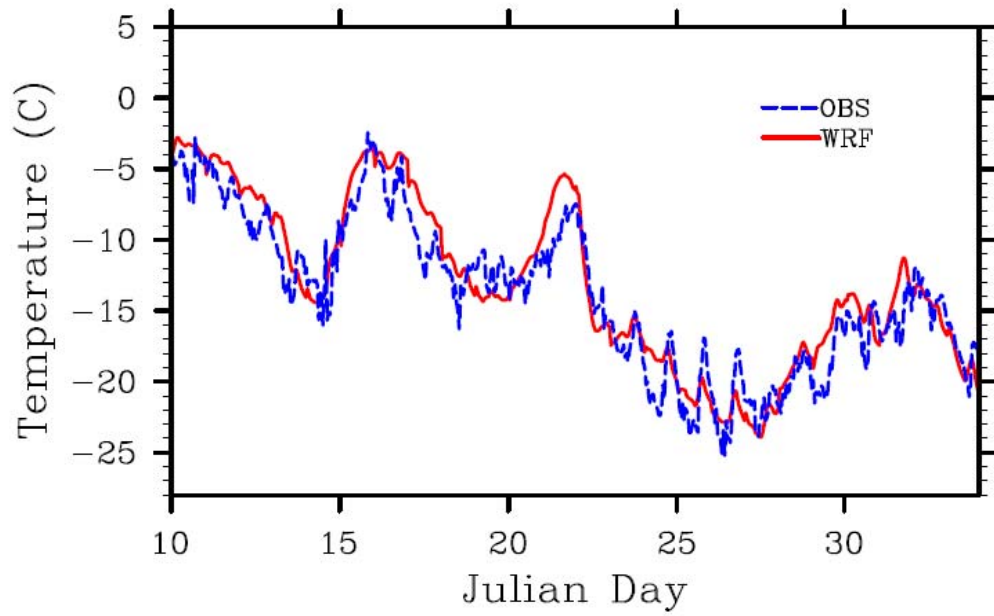


Figure 3.1 Hourly temperature ($^{\circ}\text{C}$) trends as simulated and observed. Values shown represent averages over all sites used in this study. Simulation trends are averages over all observation sites as well for direct comparison.

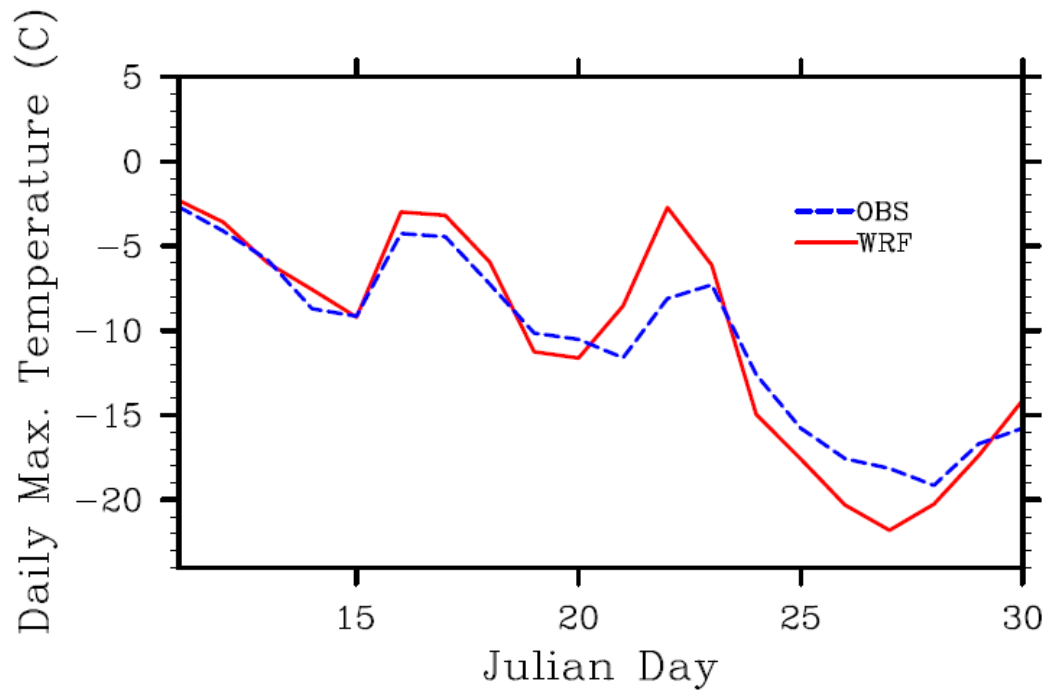


Figure 3.2 Like Fig. 3.1, but for daily maximum temperature ($^{\circ}\text{C}$).

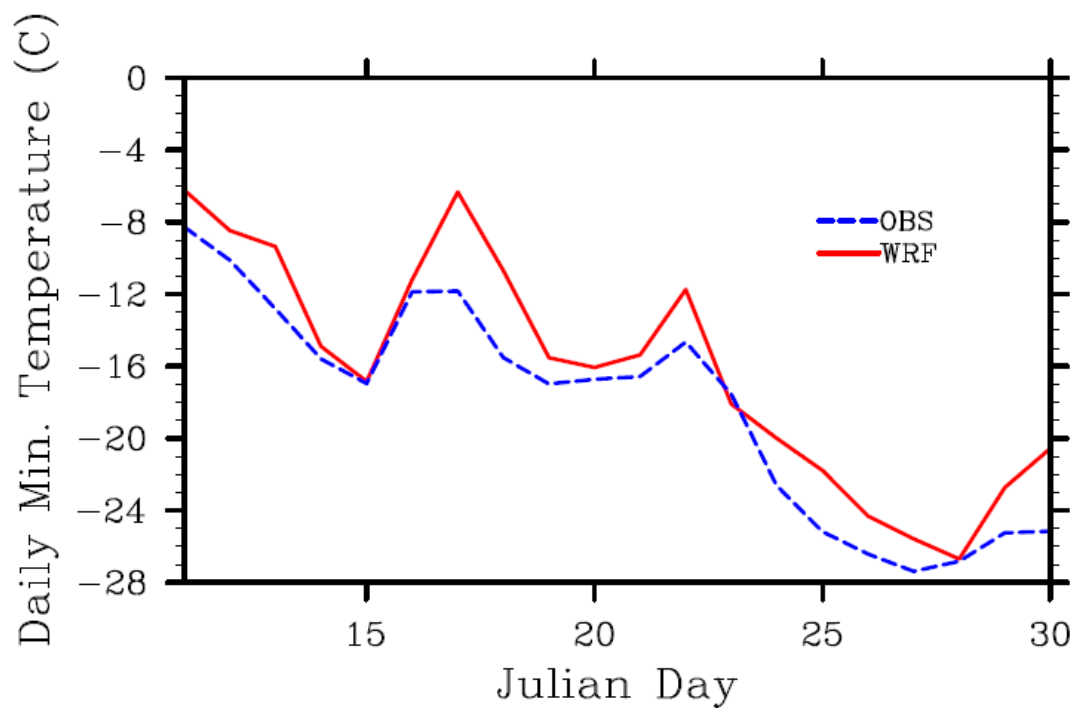


Figure 3.3 Like Fig. 3.1, but for daily minimum temperature ($^{\circ}\text{C}$).

the models used in those older studies. In this study, the hourly temperature RMSE, SDE, and bias are 0.7 K, 0.7 K, and 0.0 K, respectively. Random errors are lower than systematic errors, indicating the boundary and initial conditions lead to these errors.

In the daily temperature fluctuations (Figs. 3.2 and 3.3) WRF forecasts are delayed compared to the observations. This delay may have implications for other variables, such as cloud cover, which also has a delayed trend compared to the observational data (Fig. 3.11).

The bias scores (0.0 K, 0.1 K, and 2.1 K for hourly, daily maximum, and daily minimum, respectively) indicate systematic errors in the WRF simulation, which is likely a misinterpretation of land-surface processes, convection, and cloud cover. Hourly temperature data has a bias of 0.0 K because the negative and positive biases cancel each other out. Overestimated near-surface temperature is related to the heat and moisture exchange between the surface and atmosphere, which is likely off as a result of errors in cloudiness and hence incoming solar radiation. Note that as Table 3.1 indicates cloud existence is generally underestimated. Negative cloud cover bias is due to systematic errors in the microphysical processes (-0.1 on average). The low bias score of hourly and daily temperature, but more than an order of magnitude higher bias for maximum and minimum temperature indicate that positive and negative errors cancel each other out, i.e. WRF has some difficulties in capturing the diurnal temperature cycle for these episode. Using a similar model

setup as in this study, Mölders (2008) also found a damping of the diurnal cycle for WRF summer-simulations over Interior Alaska. This may indicate that surface fluxes are not captured well in the LSM, which can be related to a misinterpretation of the terrain height, snow cover, or downward radiation fluxes as a result of cloud cover misrepresentation. Zhong et al. (2005) found similar results over the Great Lakes region in summer for MM5 simulations with similar grid-increment than in the present study; mean values cancel out extremes and lead to overall smaller bias scores for daily averages.

The positive temperature bias has an effect on cloud-cover and dew-point temperatures. Too high temperatures allow for higher dew-point temperatures and hinder cloud formation because at higher dew-point temperature more moisture is required to reach saturation. Underestimation of cloud cover leads to overestimation of incoming solar radiation, hence altering the surface radiation budget. As a consequence further errors result in temperature, surface wind speed, and relative humidity (Zhong et al. 2005). Furthermore, underestimation of cloud cover means WRF misrepresents the cloud microphysical processes, which may lead to too low precipitation amounts.

3.2.2 Precipitation

During the entire period all precipitation fell as snow which is correctly predicted by WRF. Precipitation trends are generally appear better for the hourly

data than the daily data (Figs. 3.4 and 3.5), however these trends are somewhat misleading, so further analysis with the skill score values will be discussed in this section. Hourly precipitation trends generally follow observed values very well, with the high precipitation events captured very well across time. Daily precipitation events are generally overestimated, which is likely due to the observation network distribution within the domain. Of the 25 daily stations, seven are in or around the city of Anchorage. Consequently, model error highly depends on how well the model simulates precipitation for the Anchorage area. For the precipitation event on January 22 (Fig. 3.4), WRF overestimates the precipitation in Anchorage which leads to a large overestimation in the regional average. In other words, the distribution of precipitation observation sites does not represent the region well.

Precipitation forecasts have very small errors for the hourly data with close to zero bias, SDE, and RMSE. Daily precipitation bias, SDE, and RMSE, however, are 1.0 mm/d, 1.5 mm/d, and 2.4 mm/d, respectively (Table 3.1). Reasons for the low value bias, SDE, and RMSE for hourly data may be attributed to the region's light precipitation events for the period of study. Discussion of categorical skill scores in this section will further elaborate on this concept.

A contributing factor to the daily precipitation bias is the apparent dependency of observed precipitation to the wind speed. As wind speed increases, the rain-gauge error increases because precipitation does not fall directly into the

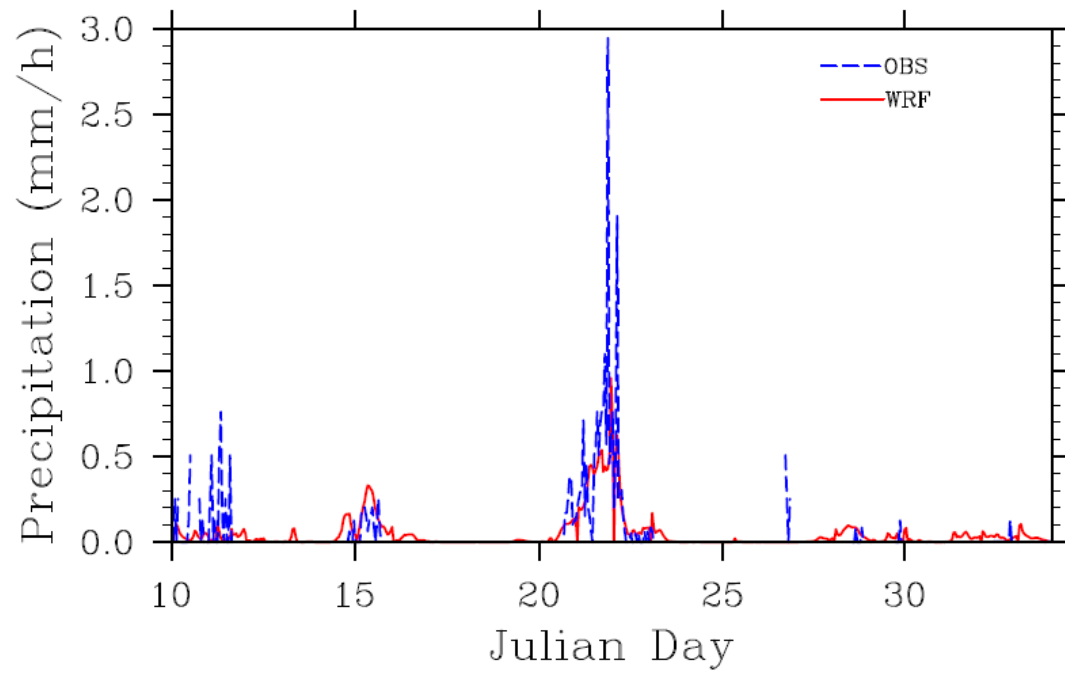


Figure 3.4 Like Fig. 3.1, but for hourly precipitation (mm/h).

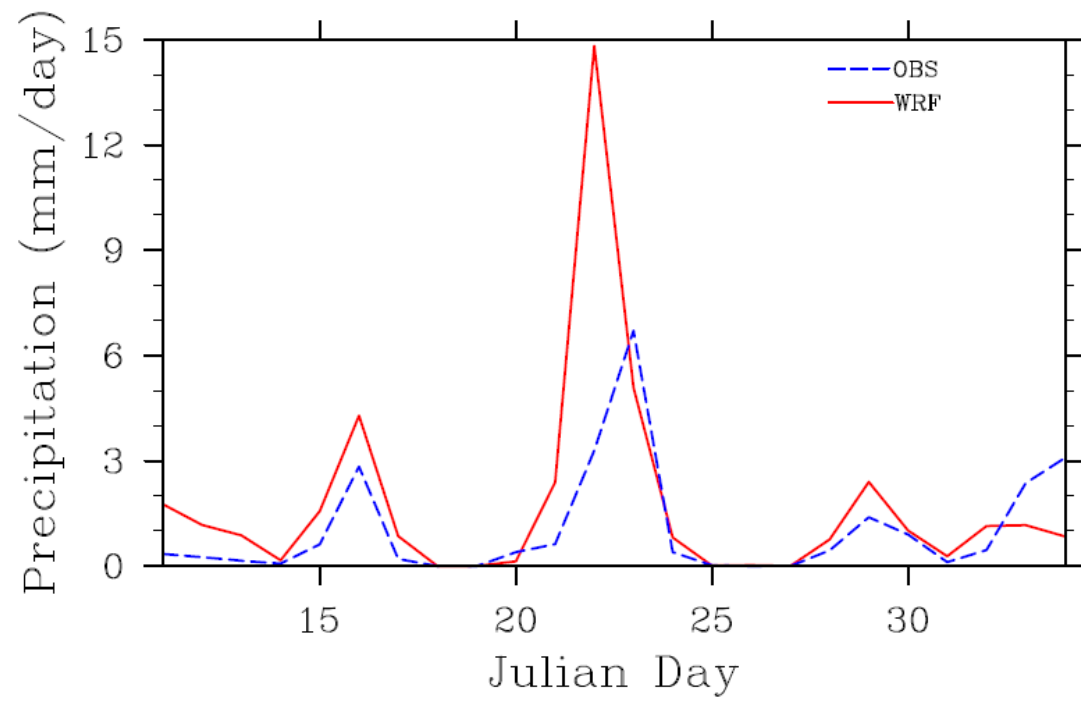


Figure 3.5 Like Fig. 3.1, but for daily precipitation (mm/d).

gauge (Dingman 1994; Yang et al. 1998). Catch deficit is larger for solid than liquid precipitation (e.g. Dingman 1994) and all precipitation occurred as snow.

Categorical scores for precipitation indicate good performance of WRF (Table 3.1). The threat scores of 0.1 mm/d for the sites with daily precipitation recordings and 0.1mm/h for those with hourly precipitation recordings are worse than the range of acceptable threat scores described in Anthes (1983; approximately 0.25 mm/d). This indicates a shortcoming in capturing the spatial distribution of precipitation events for both hourly and daily precipitation evaluations. Daily precipitation error is most influenced by random errors (with a bias of 1.0 mm/d and an SDE of 1.5 mm/d), which is likely due to the misrepresentation of the terrain as well as the catch-deficit (Fig. 3.6) and a possible misrepresentation of the domain by the location of the observing sites. The network may fail to represent the actual terrain distribution of this extremely complex terrain (cf. Fig. 2.2), for which upwind precipitation or leewind sites are in an inappropriate ratio. Average land height of the domain is 418 m, whereas the average height of the observation sites is 79m. Hence, the observation sites do not represent the domain terrain very well.

Accuracy is very high for both daily and hourly precipitation (0.9 mm/h and 0.9 mm/d, respectively). As discussed above, accuracy can be misleading because it is heavily influenced by the most common category (i.e., low or no precipitation events). With most of the domain receiving little or no precipitation events during

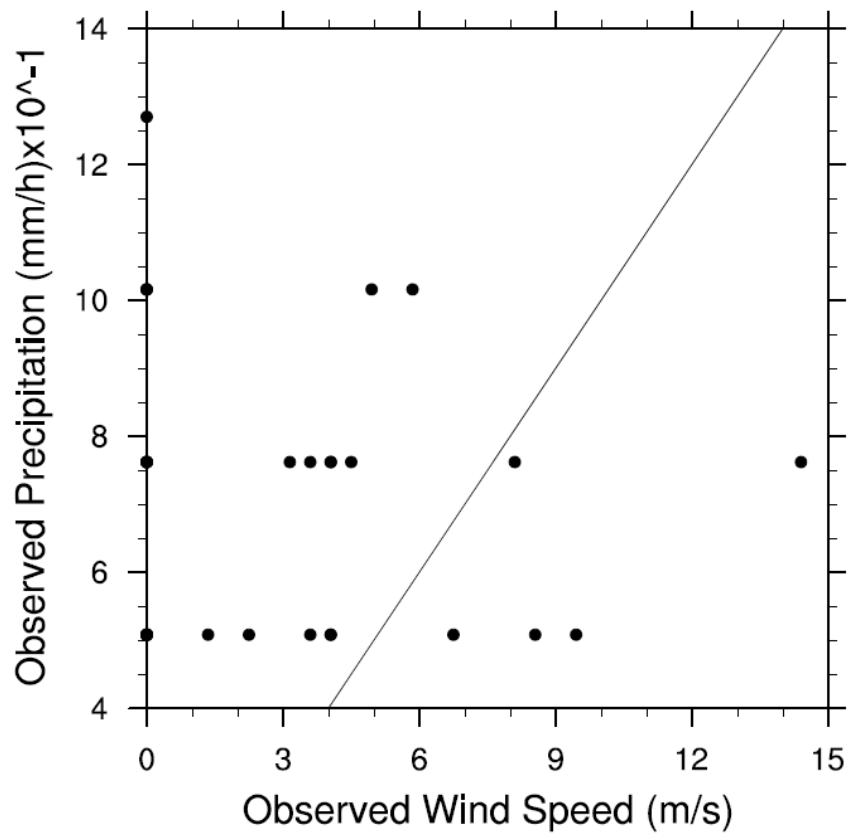


Figure 3.6 Hourly observed low-value precipitation events (mm/h) multiplied by ten (for readability) plotted against observed wind speed (m/s). The line represents a one by one line.

the majority of the time period, this accuracy value reinforces the reason hourly bias, SDE, and RMSE values are so low.

The PoD is less misleading than accuracy because it only considers correctly simulated events and incorrectly simulated events, which makes it ideal to calculate and compare with the accuracy score. If accuracy and PoD are close in value, we can expect both are fairly representative of the precipitation performance. Daily precipitation has a PoD (accuracy) score of 0.9 mm/d (0.9 mm/d) and hourly precipitation has a PoD (accuracy) score of 0.4 mm/d (0.9 m/d). This indicates that the data recorded daily had better representation of the precipitation events than the data recorded hourly.

The HSS is greater than 0.0 for both hourly and daily precipitation events (Table 3.1). This means that WRF forecasts of precipitation events exceed random chance. Based on the findings for the various scores one can conclude that the skill score values calculated for the hourly precipitation events are misleading. Data recorded hourly captured to total accumulated precipitation for an entire day, which lead to a less randomized precipitation forecast for the domain. Hourly data is collected too frequently for precipitation events that are not heavy, which lead to misrepresentation of simulation accuracy.

3.2.3 Sea-level Pressure

Overall, simulated and observed sea-level pressure differ little, showing the best temporal performance of all variables (Fig. 3.7). However, the trends vary among stations. WRF pressure trends are generally underestimated, though WRF excellently captures the timing the low-pressure system on January 22 as well as the preceding and following high-pressure systems. The underestimation of simulated data could be because the observed sites are lower than the representative WRF grid cell. The average height of the observation sites is 79 m, whereas the grid cells that represent these sites have an average height of 368 m. WRF predicts the pressure drop on January 22 and pressure peaks on January 20 and 24 with a slight delay. Slight delays in the passage of a synoptic system cause delays in other surface variables. Closer investigation shows that the underestimation of mean sea-level pressure results from WRF's overestimating the pressure gradient, which coincides with the positive wind speed bias (Table 3.1).

In general, forecasts for sites closer to the center of the model domain show better agreement with the observations than sites close to the lateral boundaries (Fig. 3.8). This is true for all quantities, however it is most easily seen in the pressure trends. With SDE scores higher than the bias (0.4 hPa and -0.0 hPa, respectively; Table 3.1) random errors associated with boundary conditions likely contribute to the overall pressure error. Another possibility is that the stations near the model domain center are near the ocean, which is a flat, low friction surface. In the case of

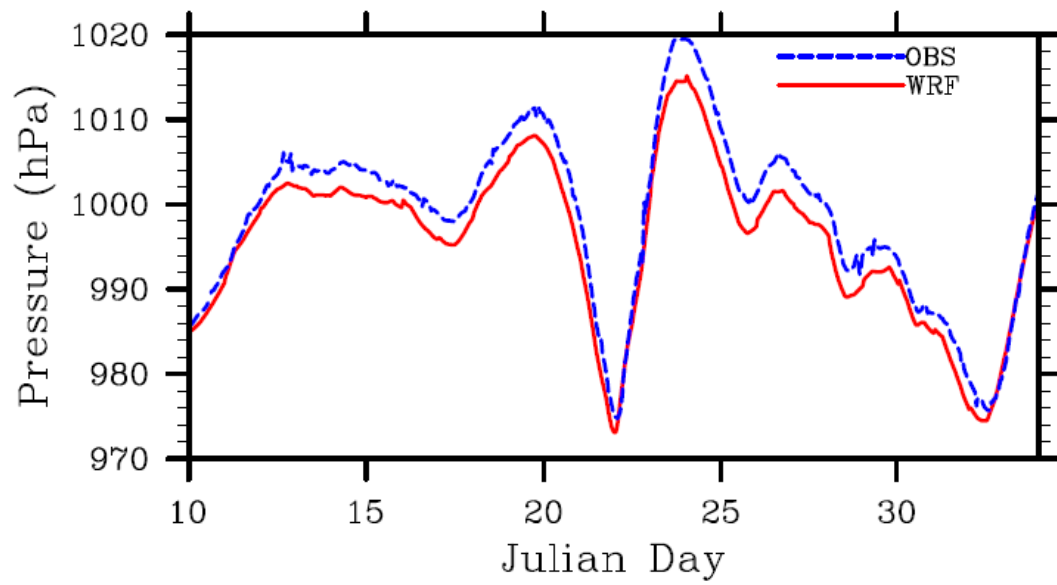


Figure 3.7 Like Fig. 3.1, but for hourly sea-level pressure (hPa).

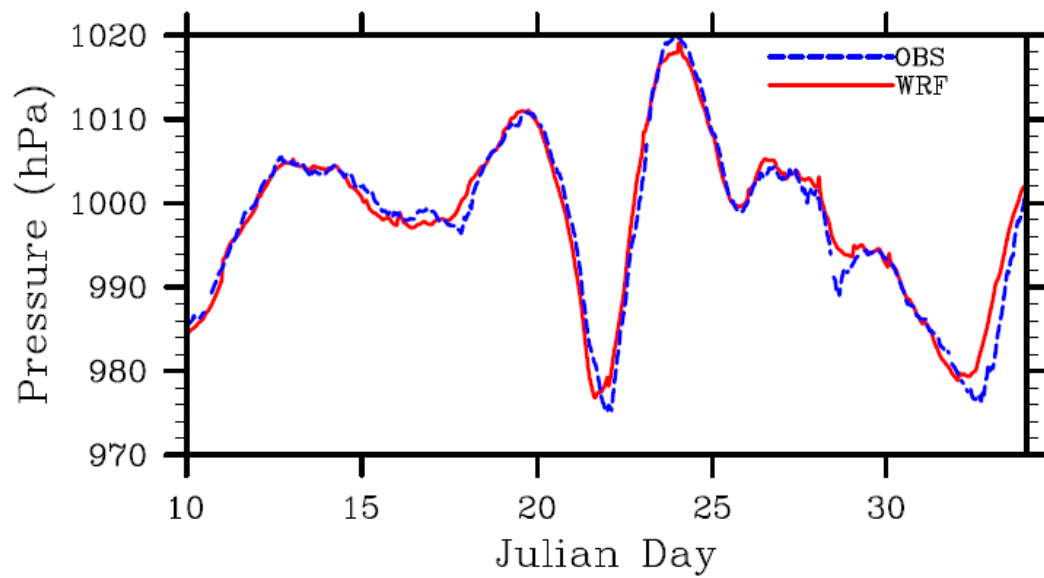


Figure 3.8.1 Hourly pressure (hPa) at the Augustine Volcano observational site.

This site is an ocean buoy just south of the volcano island, i.e. it is upwind most of the time.

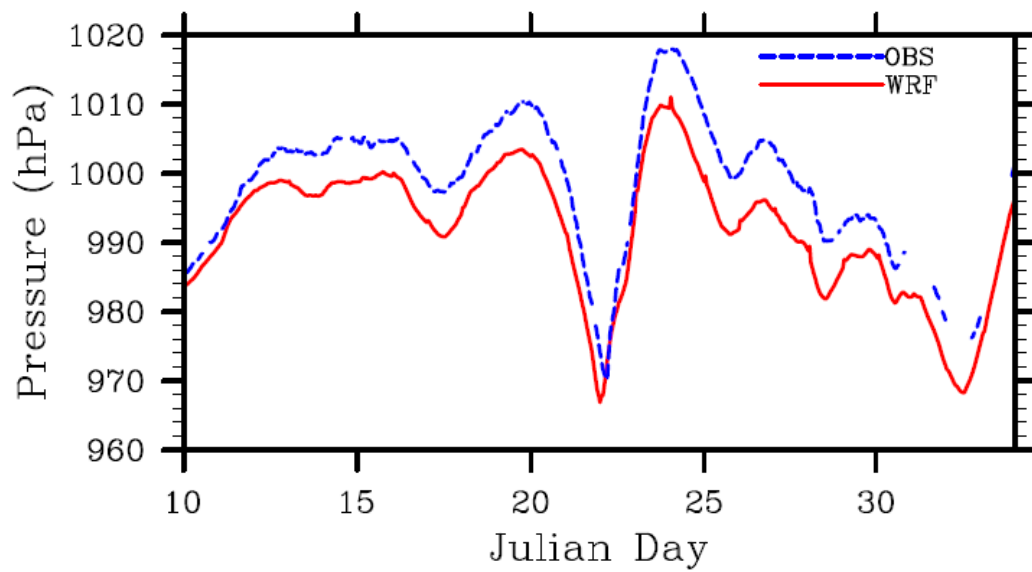


Figure 3.8.2 Like Fig. 3.8.1, but for hourly pressure (hPa) at the Palmer observing site. Palmer is approximately 350 km northeast of Augustine, and downwind of the volcano.

Fig. 3.8.1, the site is located in the middle of the domain on a buoy. Palmer, Alaska is inland, across complex terrain from the ocean (Fig. 3.8.2). WRF's misrepresentation of the terrain (due to smoothing) may lead to large errors in the pressure gradient.

The SLP-RMSE of 0.4 hPa (Table 3.1) is within the range of 0.2 to 0.8 hPa reported in previous modeling studies (e.g. Anthes et al. 1989, Colle et al. 2001, Mölders 2008). WRF simulations also seem to show improvement on the Polar MM5, which has RMSE values of 3.2 hPa according to Hines and Bromwich (2008). The SDE is much higher than the bias (0.4 hPa and -0.0 hPa, respectively; Table 3.1), indicating the random errors associated with boundary and initial conditions yield the overall error. Hence, SLP-error is mostly induced by the FNL data.

The average S_1 score for the period of interest is 11.2. This slight misrepresentation of the horizontal pressure gradient can be a factor in determining simulated wind speed. According to Anthes (1983), S_1 scores of 40-50 hPa show adequate model performance. However, he also noted that the S_1 values have been decreasing with model development. More recent studies show adequate S_1 scores for the NCEP NGM model (19; Stoss and Mullen 1995), and an extensive intercomparison model study by Gyakum et al. (1996) where S_1 values ranged between 30 and 35. Since pressure is generally underestimated, the horizontal pressure gradient is too large, hence it can be expected that wind speed is overestimated.

3.2.4 Dew-point Temperature

Discrepancies between predicted and observed dew-point temperature fluctuations (Fig. 3.9) are comparable to the differences found for temperature fluctuations (Fig. 3.1), i.e. WRF generally overestimates dew-point temperatures at all observational sites to a similar degree as it does for the air temperature, which may indicate a connection between the overestimation of simulated temperature.

Skill-scores indicate a similar discrepancy for dew-point simulations (SDE and RMSE of 0.7 K and 0.7 K, respectively) as seen in temperature forecasts (SDE and RMSE of 0.7 K and 0.7 K, respectively; Table 3.1). However, the hourly dew-point temperature forecasts have a slightly higher bias (0.1 K) than found for hourly temperature. This finding also indicates errors in low-level specific humidity. Potential reasons are misrepresentation of surface heat and moisture fluxes due to systematic errors in terrain height or snow cover. This is an improved performance from the MM5, which ranged from 1 to 2 K (e.g., Hart et al. 2003).

The most direct explanation for the overestimated dew-point is the positive temperature bias. At a given atmospheric humidity, warmer temperatures allow for more water vapor exchange between the land-surface and the atmosphere because saturation vapor pressure is higher than at relatively cooler temperatures. The SDE (0.7 K) of dew-point temperature indicates random errors that may be due to incorrect initialization of soil properties. Incorrect distribution of snow may also

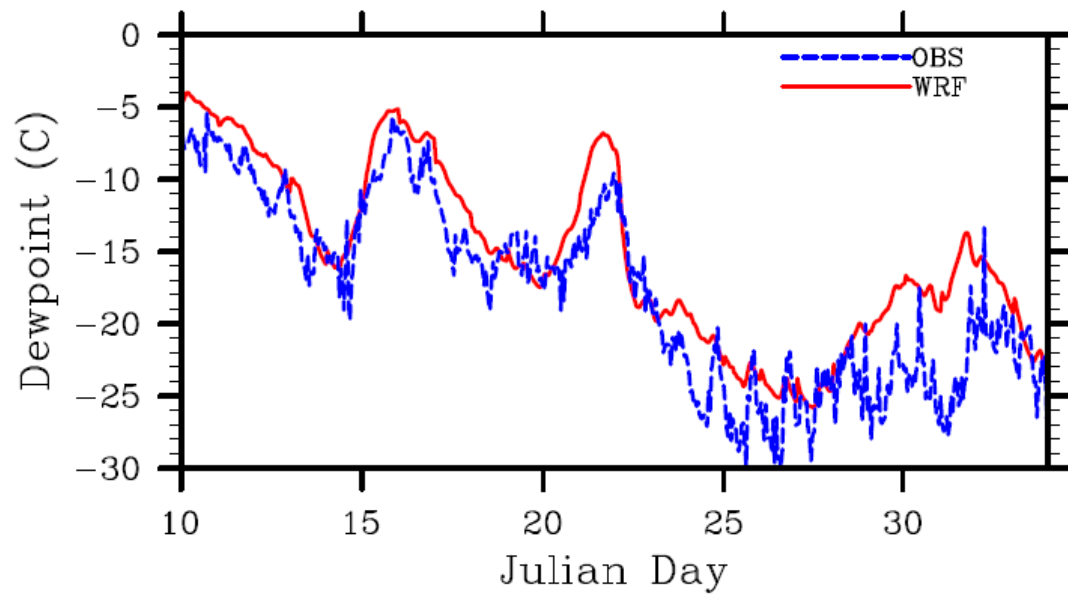


Figure 3.9 Like Fig. 3.1, but for hourly dew-point temperatures ($^{\circ}\text{C}$).

cause systematic errors that lead to an overestimation of dew-point temperature. Incorrect snow cover, namely, is a systematic misinterpretation of terrain and landscape features. If WRF misinterprets snow cover in areas of vegetation, albedo will increase/decrease if more/less of the vegetation is exposed. Lower albedo values lead to more surface heating and more sublimation of snow and an increase in surface dew-point temperature.

3.2.5 Wind Speed

Wind speed trends are difficult to generalize because the pattern is highly variable and strongly dependent on local effects (e.g. turbulence, channeling; Fig. 10). For example, observing sites in complex mountainous terrain or near forested areas experience higher turbulence than an observing site in flat terrain or with shrub vegetation.

Generally, WRF performs better for sites near the coast than locations land-inward, likely because of the low elevation and absence of complex terrain at the coast. Sites further inland tend to be embedded in mountainous terrain that can complicate the surface influence in the WRF prediction. Any misrepresentation of the terrain leads to systematic errors in wind speed. Cloud cover may also impact wind speed. During periods of transition between high pressure and low pressure in the domain, cloud cover the domain is generally dominated by broken cloud cover. It is often on these days the simulated wind speed trend varies most from the

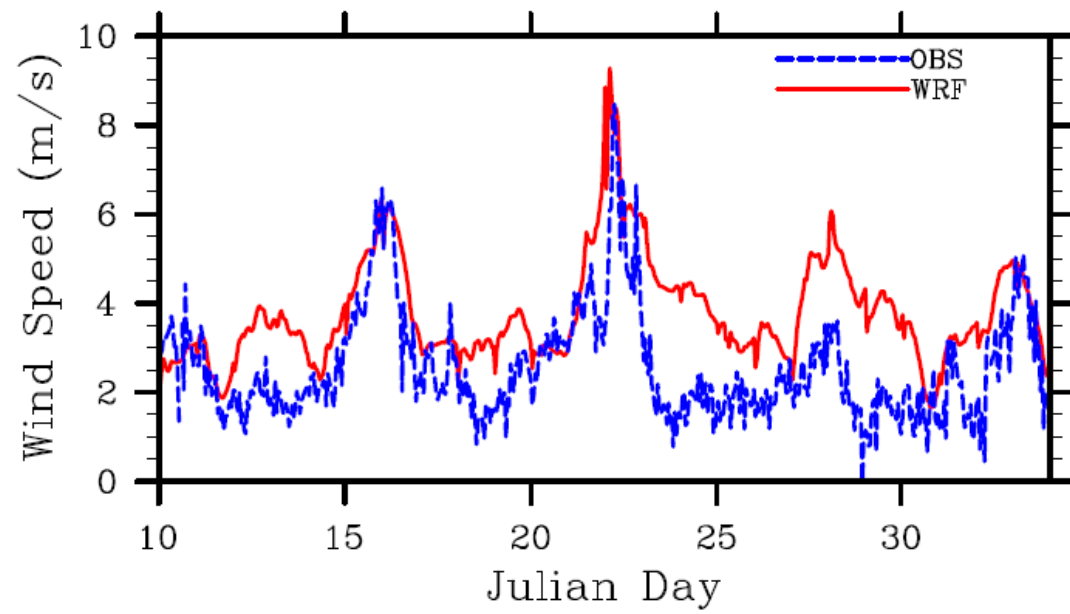


Figure 3.10 Like Fig. 3.1, but for hourly wind speed (m/s).

observed trends. Misrepresentation of cloud cover leads to incorrect surface radiation flux, which impacts surface wind speed.

The RMSE (0.5m/s) for wind speed is much lower than Zhong et al. (2005) found for MM5 for the Great Lakes region in winter (1.9 m/s) and in summer (1.8 m/s). Henderson et al. (2007) found near-surface wind speed RMSE of 1.99 m/s using the WRF model. A comparative study between the Polar MM5 and the newly developed Polar WRF show improvement in 10-m wind speed simulations, with RMSEs of 1.9 m/s and 2.1 m/s for the Polar WRF and Polar MM5, respectively (Hines and Bromwich 2008). From the discussion of the daily minimum and maximum temperatures, WRF tends to underestimate the diurnal temperature cycle, which may be due to errors in predicted convection. Incorrect prediction of vertical motion impacts the wind field for continuity reasons. Divergence related to downward motion directly affects near-surface wind speeds.

SDE and RMSE of wind-speed amount 0.4 m/s, and 0.8 m/s, respectively. WRF generally overestimates wind speed particularly during frontal passages when wind speeds are usually higher and more variable than under high pressure systems. This finding in conjunction with the findings for WRF's pressure forecasts indicates that WRF overestimates the pressure gradient. There are several reasons for WRF's overestimation of wind-speed. Obviously, terrain roughness is lower in WRF than in the real landscape. Misrepresentation of surface roughness stems from using average terrain height and the dominant land-cover type as representative for a given grid

cell. WRF, like all mesoscale models, assumes the average terrain height within a grid-cell as representative for the terrain height of the grid-cell. Consequently, channeling effects or wind shadows will not be captured, but may be reasons for observed higher or lower wind speed than predicted. Furthermore, each boundary between land-cover of different type leads to turbulence, speeding or slowing down of wind. Thus, the heterogeneity of the natural landscape results in a greater surface roughness than represented by a homogenous land-cover. Kramm et al. (1995) discussed that systematic error in wind fields may be due to different stability functions that can cause parameterization errors in wind, particularly under extreme free convection conditions. Such conditions exist, for instance, in the afternoon hours of each day and the low-pressure system on January 22 in the present study (Fig. 3.7).

The bias score for wind speed is relatively low (0.3 m/s) compared to previous forecast evaluation studies with WRF and various other models (e.g., Nutter and Manobianco 1999; Cheng and Steenburgh 2005; Zhong et al. 2005), but well fits in the range of WRF-performance for sub-arctic simulations. Mölders (2008), for instance, found that WRF slightly overestimates (~ 0.8 m/s) wind-speed, but captures the temporal mean behavior accurately for the June 2005 wildfire season in Interior Alaska. Henderson et al. (2007) reported mean bias of about 0.33 m/s at 0000 UTC and ~ 0.36 m/s at 1200 UTC for a mesoscale- α study with WRF over Siberia. Nutter and Manobianco (1999), Cheng and Steenburgh (2005), and Zhong et al. (2005)

found wind speed biases of ± 2 m/s (Florida, NCEP model winter-time evaluation), 0.5 m/s (Western United States region, WRF and Eta summer-time evaluation), and 0.5 m/s (Great Lakes region, MM5 winter-time evaluation), respectively.

3.2.6 Cloud Existence

Temporal evolution (Fig. 3.11) of cloud existence indicates that WRF generally captured cloud events, but there tends to be a delay in cloud onset, particularly at the end of our study period. One reason for this delay is related to the restarts. WRF begins each simulation with no cloud cover and no precipitation, so some time is needed for clouds to form. Another reason is that the pressure system simulation trends are generally delayed or hastened compared with observing sites for the entire domain. Low-pressure systems are associated with cloud cover; thus a delay in low-pressure systems moving in causes a delay in cloud cover. Also, overestimating near-surface temperature likely contributes to error in cloud cover as higher specific humidity is required for onset of cloud formation.

Cloud existence has a negative bias overall (-0.1; Table 3.1). RMSE and SDE have values of 0.8 and 0.4, respectively. This means that random errors associated with the boundary and initial conditions are the primary cause of cloud existence error.

Accuracy and threat score of cloud existence amount to 0.6 and 0.4, respectively. It is important to note that threat scores are lower for rare events than

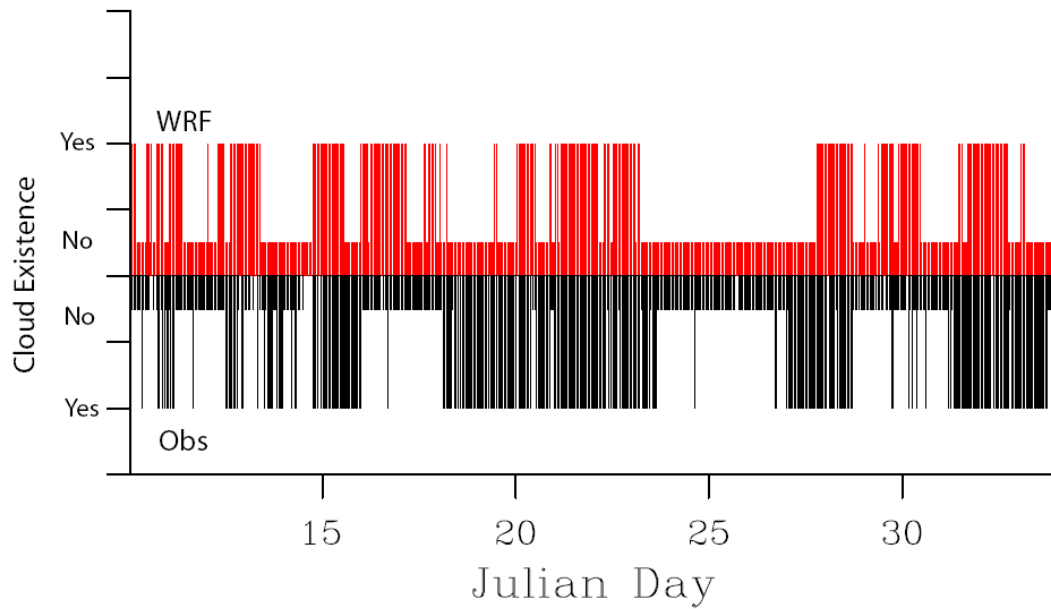


Figure 3.11 Cloud cover over for Soldotna, Alaska, approximately 150km downwind of Augustine. This station best represents the cloud existence trends for the rest of the stations in this study with cloud cover reported. Lines going up represent WRF simulated cloud existence and lines going down represent observed cloud existence. No lines indicate missing data.

high frequency events because any “misses” lower the score. This means that overcast and clear days will generally give higher values of the threat and accuracy scores. For partly cloudy events, “misses” are punished in the score for threat and accuracy. According to the Heidke-skill score ($HSS = 0.1$), correct WRF cloud simulations are better than random chance (Table 3.1). The fact that dew-point temperature has a positive bias and cloud existence has a negative bias, can be interpreted that WRF predicts atmospheric moisture content sufficiently well, but the microphysical processes are simulated slightly less precisely.

3.3 Conclusions from the Evaluation

The results show that the WRF forecasts adequately represent the synoptic situation. WRF’s performance is evaluated by observations from 17 sites with hourly reported data and 26 sites with daily reported data. Overall, WRF showed very good performance skill when compared with previous model evaluation studies of WRF and other mesoscale models. Though it may not always simulate the values correctly, it captures the trends very well (i.e., precisely). In general, WRF tends to overestimate dew-point temperature, wind speed, precipitation, and 2m-air temperature; and generally underestimates sea-level pressure and cloud presence for the episode considered here.

Generally, WRF has some difficulties capturing the width of the diurnal cycle. Skill-scores indicate this difficulty results from random errors rather than

systematic errors. Precipitation has large, but acceptable errors when evaluated by daily accumulated data. Errors in the daily precipitation forecasts stem from both random and systematic errors associated with catch-deficit and poor regional representation by available observation sites. Sea-level pressure showed good representation of the pressure systems for the region. The generally better forecasts of sea-level pressure for stations in the center of the region and the higher SDE than bias indicate that random errors associated with the boundary conditions mainly contribute to SLP-errors. This means that some error is imported from the driving data. Dew-point temperature error is generally random; however, it can also be explained by the systematic misrepresentation of land-cover and terrain height as a result of smoothing terrain and homogenizing land-cover type. Wind-speed errors, according to skill-scores, are also due to random errors, i.e. boundary conditions. However, the systematic overestimation also indicates that misrepresentation of terrain height and surface heterogeneity both contribute to the overall error; model performance is better in coastal areas than for stations inland that are strongly influenced by terrain-induced turbulence. Generally, cloud cover is delayed and hence slightly underestimated in the forecasts, which is a combined result from the slight delay in the onset of low-pressure systems (boundary conditions) and starting with zero cloud and precipitation particles.

We can conclude from these findings that WRF can adequately capture the synoptic situation of the domain during a volcano eruption. Simulations of this

performance can be used to further determine the impact of the 2006 Augustine Volcano eruption on local, daily weather for the domain.

4. Augustine Eruption Effects

4.1 General Remarks

For this study, two domains are considered when analyzing the Augustine Volcano's influence on weather. Domain A is the large domain, which includes 140x140 grid cells (i.e., the outermost nine grid cells from the simulation domain are not considered to exclude effects from lateral boundaries in the limited area model). Domain B is a smaller area (51x51 grid cells) centered over the area downwind of Augustine (Fig. 4.1). In this paper, any reference to *significant* changes implies the changes are *statistically significant*, as determined by ANOVA.

4.2 Determining the Error for the ANOVA

The linear ANOVA model is expressed in terms of the Sum of Squares and the error (Montgomery 1976)

$$SS_T = SS_E + \sum_i \sum_j \sum_k \sum_l SS_{ijkl} \quad (4.1)$$

where i , j , k , and l represent the two levels for the heat, water vapor, aerosol, and ash fall factors, respectively. For higher-order factorial designs, the square sum of errors SS_E is defined as the sum of all treatments that have very small sum of square values (Montgomery 1976). To determine which factors fall into this category, normal probability plots are generated across the domain (Fig. 4.2). For example, the estimate for heat release is defined as

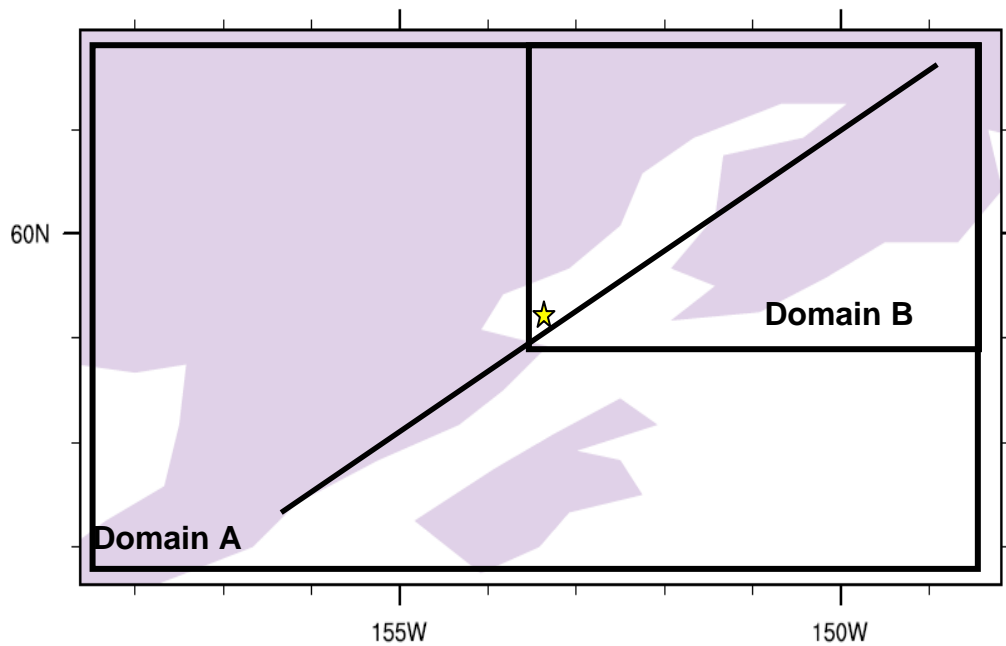


Figure 4.1 Model domain with overlaying domain A, and domain B as used for testing the area significantly impacted by the Augustine eruption. Domain A is the entire model domain with exception of the five grid cells closest to the boundary (to avoid model boundary error issues). Domain B is a subsection of Domain A, the area that was generally downwind of Augustine during the period of interest. The star shows the location of the Augustine Volcano in the center of the domain and the line represents the location of a vertical cross section that will be used in future plots.

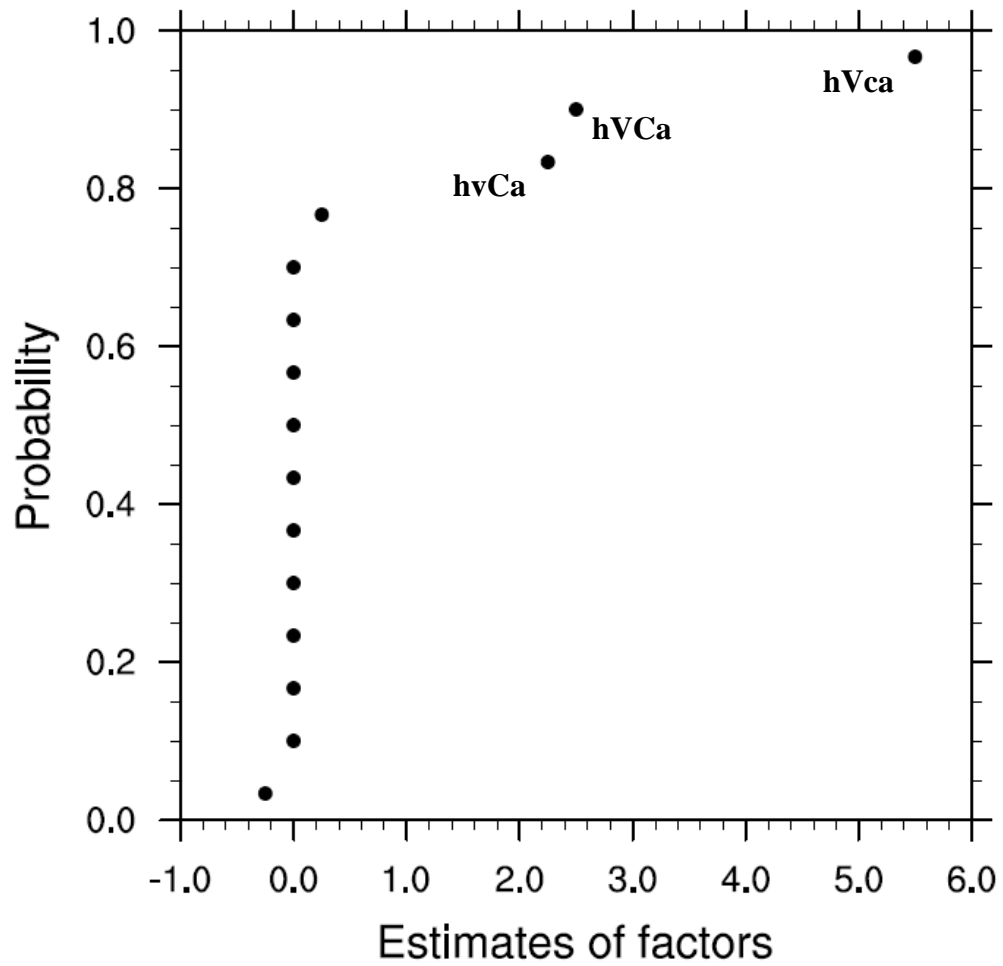


Figure 4.2 Normal Probability plot for January 15, 2006. Note that plots for all other days look similar (therefore not shown).

$$E_{Hvca} = \frac{1}{n2^4} (\text{Contrast}_{Hvca}) \quad (4.2)$$

where n is the number of replicates, which is one for this study (as discussed in chapter 2, this is commonly done for higher order ANOVA designs for simplicity). Each treatment's estimate is ranked in order from lowest value to highest value, and then the probability of each value's occurrence is calculated based on (Montgomery 1976)

$$P_m = \frac{(m - 0.5)}{(2^k - 1)} \quad (4.3)$$

where m is the rank of the value when ordered from lowest to highest. For higher-order ANOVA designs, it is estimated that all factors that do not fall in a linear pattern are not significant and, thus, are considered error (Montgomery 1976). For this study, normal probability plots are generated for each day, so treatments that are out of place at any time during the period are considered significant. All other treatments are used to determine the error. Analysis shows that the sum of squares for the error for this study can be determined using

$$\begin{aligned} SS_E = & SS_{hVcA} + SS_{HvcA} + SS_{hvCA} + SS_{HvCa} + SS_{HVCA} + SS_{HVcA} \\ & + SS_{HvCA} + SS_{hVCA} + SS_{HVCA} \end{aligned} \quad (4.4)$$

4.3 Results and Discussion

Days with significant volcanic influences (according to the ANOVA) are analyzed over domain A and domain B to see how far reaching the significant

impacts of the volcano on weather may have been. For days where the volcano significantly impacts domain A, it also significantly impacts domain B (Table 4.1). It is important to note that the volcano results discussed in this study is the result of the hypothetical situation discussed in chapter 2. It does not necessarily represent what actually occurred during the actual Augustine eruption. For comparison to the actual eruption, the height of volcano-simulated material can be analyzed by plotting water vapor vertical transport. Not considering explosive trajectory, emissions from the volcano are lifted as high as approximately 600 hPa. In this scenario, CCN/IN sized particulates from the volcano are estimated from previous eruptions as discussed in chapter 2. CCN/IN particles provide a surface for nucleation of water/ice drops to form under favorable synoptic conditions (i.e., adequate moisture source and lift).

The days with the most significant interference from Augustine are at the end of the period, from January 24 through February 2. During this time, there are widespread cloud cover and precipitation events across domain A. Augustine's activity was past the eruption phase and had entered its effusive phase, which means it released a steady stream of particulates into the atmosphere rather than large, short, eruptive bursts of particles (cf. Fig. 2.3; Dehn pers. communication 2007). The days with the least amount of significant interference of the volcanic activity with local weather are near the beginning and middle of the period (January 10, 11, 12, 15, 17, and 21). At the beginning of the period, a high-pressure system dominated the

Table 4.1 Domain B total treatment value minus control on January 25, 2006. Non-significant values are not reported. The variables considered are surface temperature (T), precipitation (P), water vapor mixing ratio (q_v), cloud ice mixing ratio (q_i), cloud water mixing ratio (q_c), and vertical velocity (w), respectively.

Simulation	T (K)	P (mm/h)	q_v (g/kg)	q_i (g/kg)	q_c (g/kg)	w (m/s)
hvcA						
hVca	19.0	1.1	0.01	0.0	0.0	0.11
Hvca	-19.0	0.1	-0.001	0.0	-1.07×10^{-6}	-0.18
hvCa	0.0	0.0	0.0	0.0	0.0	0.0
hVCa		1.1	0.01	0.0	0.0	0.15
HvCa		0.1	-0.001	0.0	-1.1×10^{-6}	-0.18
hvCA		0.0	0.0	0.0	0.0	0.0
HVca		1.2	0.01	0.0	0.0	0.02
hVcA						
HvcA						
HVCa			0.01	-1.4×10^{-8}	0.0	0.05
HVcA		1.2				
HvCA						
hVCA						
HVCA						

region. It was not until January 23 that a low-pressure system developed in the region, bringing cloud cover and precipitation to the region.

The clustering of numerous significant treatments during the end of the period of study could be the result of two scenarios; (1) the period had the best synoptic condition to detect changes (i.e., uniform, widespread cloud cover and precipitation), and/or (2) the continuous phase of the Augustine eruption had the most significant interactions with the regional weather.

On January 17, Augustine erupted severely sending a plume of ash 13 km above sea-level (Power et al. 2006), however, significant volcanic effects on this day for domain A is very low (Table 4.2); likely due to the clear, stable atmospheric conditions upwind of the volcano. During the days with widespread cloud cover, frequent precipitation events, and concurrent eruption, significant volcanic influences on cloud and precipitation formation are most frequent. January 21 and 22 had widespread precipitation events and overcast skies across most of the domain (Fig. 3.5), yet weather on these days experiences very few significant effects of the volcano, even though the volcano is relatively active on those days for our hypothetical scenario (Fig. 2.3). The end of the period also has widespread precipitation events, though most days have more significant volcanic influences than those during early period precipitation events. Therefore, the continuous phase of the volcanic eruption has a larger impact on daily, regional weather than the explosive phase did at the beginning of the period.

Table 4.2.1 Atmospheric variables with significant volcanic influences for domain A (indicated with an X) for January 10, 2006. The variables considered are surface temperature (T), precipitation (P), water vapor mixing ratio (q_v), cloud ice mixing ratio (q_i), cloud water mixing ratio (q_c), and vertical velocity (w), respectively.

	T	P	q_v	q_i	q_c	w
hvcA						
hVca		X	X	X		X
Hvca						
hvCa	X	X		X	X	
hVCa	X	X	X	X	X	X
HvCa						
hvCA						
HVca						
hVcA						
HvcA						
HVCa						
HVcA						
HvCA						
hVCA						
HVCA						

Table 4.2.2 Same as 4.2.1, but for January 11.

	T	P	q_v	q_i	q_c	w
hvcA						
hVca					X	
Hvca						
hvCa						
hVCa					X	
HvCa						
hvCA						
HVca						
hVcA						
HvcA						
HVCa						
HVcA						
HvCA						
hVCA						
HVCA						

Table 4.2.3 Same as 4.2.1, but for January 12.

	T	P	q_v	q_i	q_c	w
hvcA						
hVca		X	X	X	X	X
Hvca						
hvCa	X	X		X	X	X
hVCa	X	X	X	X	X	X
HvCa						
hvCA						
HVca						
hVcA						
HvcA						
HVCa						
HVcA						
HvCA						
hVCA						
HVCA						

Table 4.2.4 Same as 4.2.1, but for January 15, 2006.

	T	P	q_v	q_i	q_c	w
hvcA						
hVca	X	X	X	X	X	X
Hvca	X	X				
hvCa					X	X
hVCa			X	X		X
HvCa						
hvCA						
HVca	X					
hVcA						
HvcA						
HVCa		X				
HVcA						
HvCA						
hVCA						
HVCA						

Table 4.2.5 Same as 4.2.1, but for January 17, 2006.

	T	P	q_v	q_i	q_c	w
hvcA		X		X		
hVca		X	X	X	X	X
Hvca						
hvCa		X	X		X	X
hVCa		X	X	X	X	
HvCa						
hvCA						
HVca						
hVcA						
HvcA						
HVCa						
HVcA						
HvCA						
hVCA						
HVCA						

Table 4.2.6 Same as 4.2.1, but for January 21, 2006.

	T	P	q_v	q_i	q_c	w
hvcA						
hVca		X		X		
Hvca	X	X				
hvCa	X	X				
hVCa		X				
HvCa		X				
hvCA	X	X				
HVca	X	X				
hVcA						
HvcA						
HVCa	X	X				
HVcA						
HvCA						
hVCA						
HVCA						

In the following, a general overview on the impacts found is given. Days with the significant impact of volcanic effects and/or significant interaction of volcanic effects will be discussed in detail later in this chapter.

4.3.1 Augustine Volcano Effects

Water vapor release has the single largest impact on the weather (Tables 4.1, 4.3, 4.4, and 4.5). Volcanic water vapor release has little impact locally when the regional weather is dry and calm when concurrently there is little to no volcanic activity. This finding can be explained by the higher concentrations of water vapor that lead to condensation and increased cloud cover. Clouds lead to warming of the near-surface air temperatures under the wintertime conditions in Polar Regions. Cloud cover drives surface temperature for the domain because radiative cooling dominates heat exchange at the surface compared to incoming solar radiation due to limited daytime hours. Furthermore, latent heat released during condensation and deposition of water vapor increases air temperature. In response to the volcanic water vapor release, precipitation generally increases (totaling as much as 51.7 mm/h) significantly on most days, because under the atmospheric conditions of these days an increase in water vapor means super-saturation can be more easily reached and/or more water vapor is available for condensation/deposition, which increases the radii of hydrometeors.

Table 4.3 Same as 4.1 but for February 2, 2006.

Simulation	T (K)	P (mm/h)	q_v (g/kg)	q_i (g/kg)	q_c (g/kg)	w (m/s)
hvcA						
hVca	21.0	49.1	0.02	0.0	0.003	0.03
Hvca	707.0	-14.0	9.9×10^{-5}	-4.3×10^{-6}	-0.001	1.4
hvCa	3.0		-0.0004	0.0	6.6×10^{-5}	-0.12
hVCa		51.7	0.02	0.0	0.003	-0.16
HvCa	9.0	0.05	9.9×10^{-5}	-4.3×10^{-6}	-0.001	1.4
hvCA		-1.1	-0.0004	0.0	6.6×10^{-5}	-0.12
HVca	719.0	39.4	0.02	-3.5×10^{-6}	0.003	2.15
hVcA						
HvcA						
HVCa		39.9	0.02	-3.4×10^{-6}	0.003	2.1
HVcA						
HvCA						
hVCA						
HVCA						

Table 4.4 Same as 4.1 but for January 30, 2006.

Simulation	T (K)	P (mm/h)	q_v (g/kg)	q_i (g/kg)	q_c (g/kg)	w (m/s)
hvcA						
hVca						
Hvca	15.0	-9.5	-0.0001	0.0	-0.0001	0.98
hvCa	0.0					0.0
hVCa		41.9		0.0	1.2×10^{-5}	-0.37
HvCa	15.0	-9.5		0.0	-0.0001	0.98
hvCA	0.0					0.0
HVca	28.0	32.1	0.005	0.0	-4.8×10^{-5}	0.14
hVcA	47.0			0.0	-2.7×10^{-5}	-0.14
HvcA						
HVCa						
HVcA	28.0	32.1	0.005	0.0	-4.8×10^{-5}	0.14
HvCA						
hVCA						
HVCA						

Table 4.5 Same as 4.1 but for January 29, 2006.

Simulation	T (K)	P (mm/h)	q_v (g/kg)	q_i (g/kg)	q_c (g/kg)	w (m/s)
hvcA						
hVca	76.0	6.6	-0.001	0	-0.0002	-1.18
Hvca			-0.007	0.0	-0.0004	-2.25
hvCa	0.0		0.0	0.0	0.0	0.0
hVCa	22.0		-0.004	0.0	-0.0003	-2.01
HvCa	-20.0		-0.007	0.0	-0.0004	-2.25
hvCA	0.0		0.0	0.0	0.0	0.0
HVca			0.002	0.0	-0.0001	0.12
hVcA						
HvcA						
HVCa	18.0	11.9	-0.001	0.0	-0.0003	-1.79
HVcA						
HvCA						
hVCA						
HVCA						

Volcanic heat release has an impact on temperature for domain A. It has significance as an individual treatment, but tends to be significant more often when coupled with volcanic water vapor release or aerosol release (i.e., the aHVc and aHvC treatments). Precipitation change is significant for the majority of the days; however, it is significant most frequently during the continuous eruption phase (Tables 4.1, 4.3, 4.4, and 4.5). Generally, as the amount of precipitation per event increases, cloud ice water mixing ratio increases and cloud water mixing ratio decreases (Table 4.1).

Aerosol effects are more often significantly associated with water vapor in interaction treatments than aerosol effects alone (Tables 4.1, 4.3, 4.4, 4.5). Since the volcanic aerosol release is assumed to act as CCNs and INs, aerosol release also impacts cloud microphysical processes on cloudy days. Additional CCNs lead to an increase in cloud particle number, thus a decrease in cloud particle size. Smaller droplets lead to less overall precipitation for the reasons outlined in chapter 2, section 2.1.

Changes in precipitation can occur as a result of three mechanisms that will be discussed in this study: 1) increased surface heating leads to more buoyant air near the surface, which increases vertical velocity that leads to cooling, hence formation of hydrometeors is enhanced (Fig4.3a), 2) shifting hydrometeors from liquid to ice can also enhance precipitation, whereas a decrease in ice particles hinders precipitation growth because the shape of ice particles allows for more

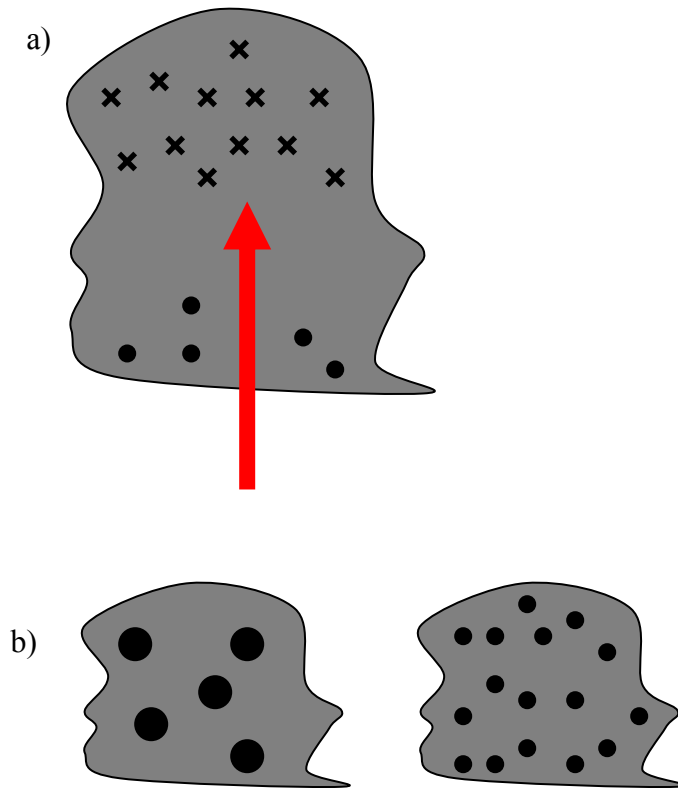


Figure 4.3 Schematic of the microphysical processes that drive changes in precipitation. Part a) shows that vertical motion can increase the ice particles through adiabatic cooling, which can occur through buoyant energy caused by surface heating. Part b) shows that increasing CCN/IN provides more surface area for available water vapor to condense on, leading to more numerous, smaller hydrometeors. Larger hydrometeors can more easily overcome gravity to lead to surface precipitation.

efficient growth (Pruppacher and Klett 1997), and 3) increasing the CCN/IN increases the number of particles, which decreases the size of the particles because there is more surface area for available water vapor to condense on, effectively decreasing precipitation (Fig 4.3b). In this study, changes in vertical velocity and water/ice particle mixing ratios will be examined to determine cause in precipitation changes as a result of volcano eruption influences.

Ash fall only significantly impacts atmospheric variables when combined with aerosols for the domain A (Table 4.2), with stronger significant impacts in domain B, downwind of Augustine. This finding indicates that the temperature-albedo feedback effect alone does not significantly impact local weather under the hypothetical volcano eruption scenario. In January, the ground is snow-covered. A layer of ash fall is darker in color than the white snow. Darker colors have a smaller albedo, which means it absorbs more sunlight than the white snow with a higher albedo. As albedo decreases, temperature of the surface increases because more sunlight is absorbed. Increasing temperature will eventually lead to melting snow, effectively increasing the surface temperature even more because more dark soil is exposed (Fig. 4.4). This is the temperature-albedo feedback, which will be referred to again in this paper. Ash fall would need to decrease albedo drastically to significantly increase the surface temperature enough to create enough vertical motion (through buoyant air at the warming surface as discussed earlier) to aid in precipitation development.

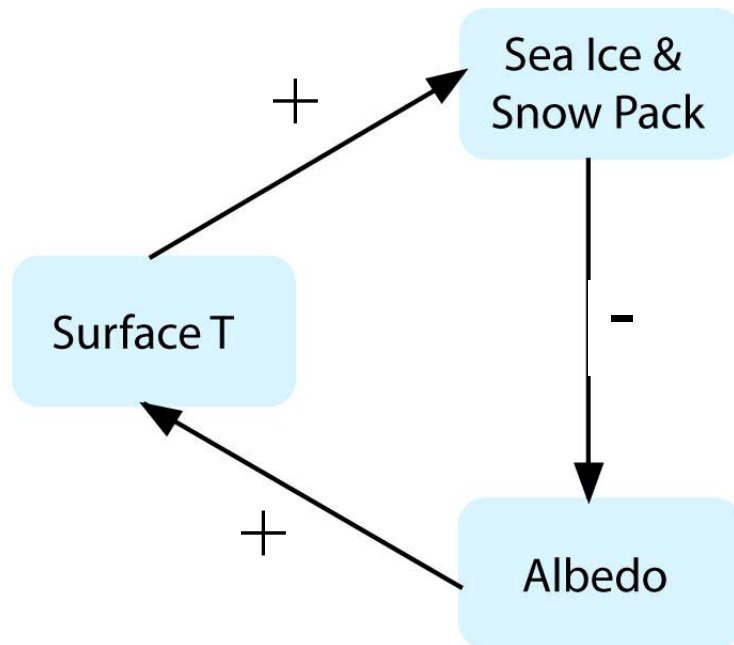


Figure 4.4 Schematic representation of the temperature-albedo feedback mechanism. Decreasing the albedo of the surface via ash fall leads to an increase in surface temperature, which can lead to a melting snow pack, effectively increasing the albedo even more.

4.3.2 January 25

On January 25, Augustine was in its last days of the explosive phase, where eruptions were still short, large bursts (Dehn pers. communication 2007). Pressure dropped due to an approaching low-pressure system, hence cloud cover and precipitation events were increasing across the domain (c.f. Fig. 3.7).

For all quantities examined (except temperature), statistically significant factors for ANOVA domain A are the single release of either 1) water vapor (hVac), 2) heat (Hvac), 3) aerosol (hvCa), and the concurrent release of 4) water vapor and aerosols (hVca), 5) heat and aerosols (HVca), 6) aerosols and ash fall (hvCA), and 7) water vapor and heat (HVca). Simultaneous release of heat, water vapor and aerosols causes significant changes in all quantities investigated except for precipitation and temperature (Table 4.6). For release of heat and concurrent ash fall, only precipitation experiences significant changes (Table 4.6).

The sole release of volcanic water vapor (simulation hVca) increased temperature and precipitation significantly by as much as 0.05 K and 0.003 mm/h for domain B (Fig. 4.5 and 4.6). If the atmospheric conditions are favorable at the surface, condensation occurs due to the additional available water vapor, and increases near-surface air temperature. The elevated water vapor also causes an increase in cloud-water mixing ratios and vertical velocity (Fig. 4.7). The water vapor condenses on available CCNs and INs and, generally, the resulting cloud and

Table 4.6 ANOVA summary table for precipitation on January 25, 2006 for the domain B. F values of 95% significance are used. Bold values are statistically significant.

Simulation	MS	F value
hvcA	4.6×10^{-8}	8.1×10^{-5}
hVca	4.91	8761.26
Hvca	0.038	68.96
hvCa	.00016	0.29
hVCa	0.00017	0.30
HvCa	0.0030	5.33
hvCA	0.0030	5.33
HVca	0.0016	2.91
hVcA	9.31×10^{-10}	1.67×10^{-6}
HvcA	0.0	0.0
HVCa	0.0030	5.33
HVcA	0.0	0.0
HvCA	0.0	1.7×10^{-6}
hVCA	9.3×10^{-10}	1.7×10^{-6}
HVCA	0.0	0.0

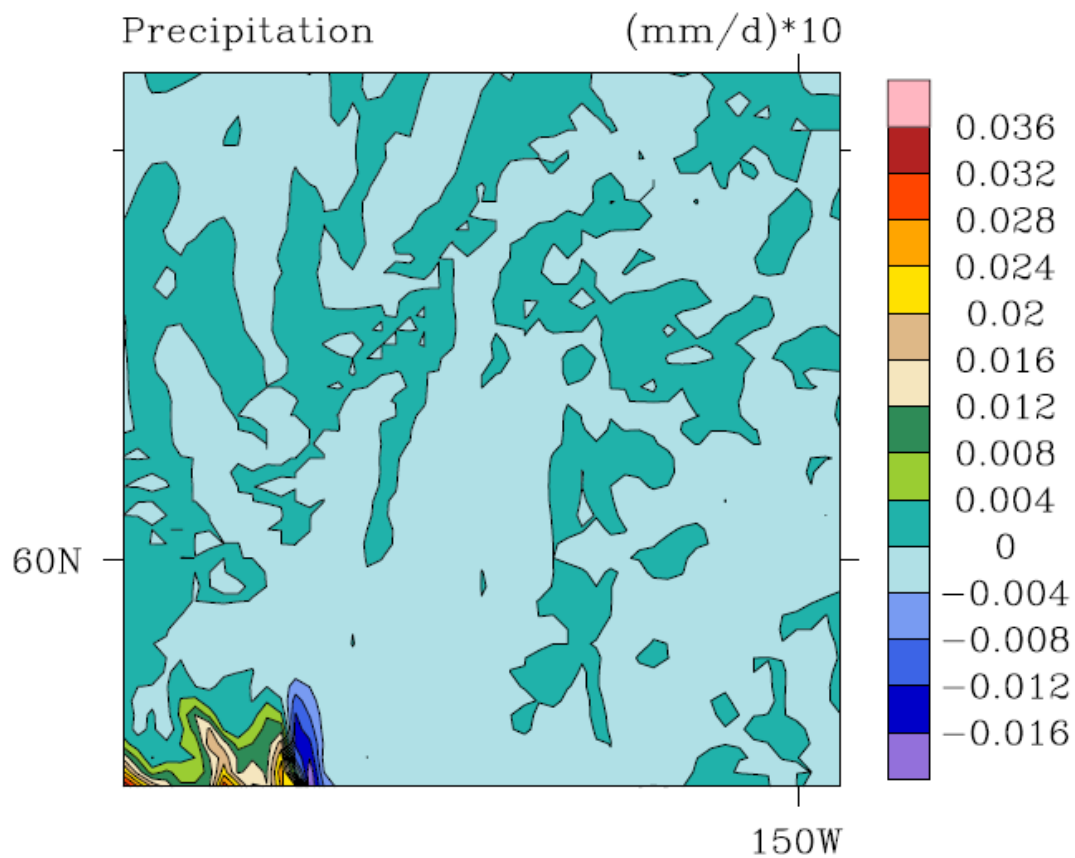


Figure 4.5 Difference between domain B accumulated precipitation for the water vapor simulation (hVca) minus the control run (hvca) for January 25.

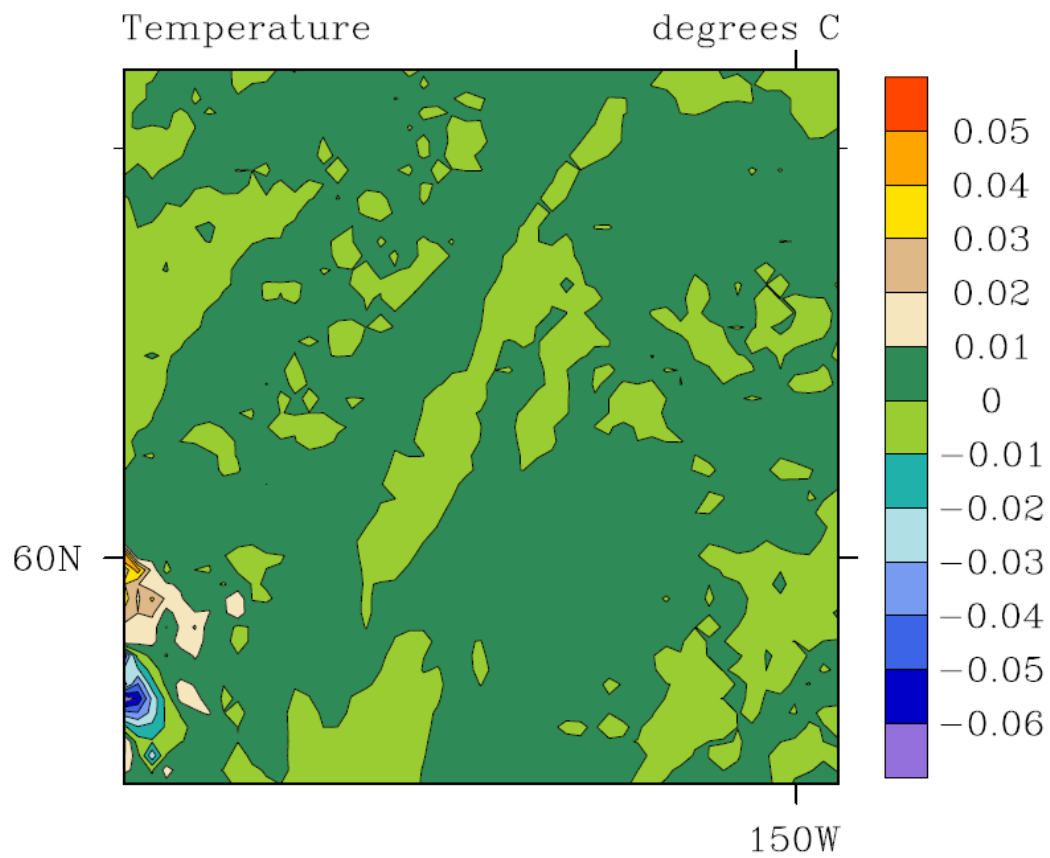


Figure 4.6 Difference in daily averaged surface temperature between domain B water vapor simulation (hVca) and the control run (hvca) for January 25.

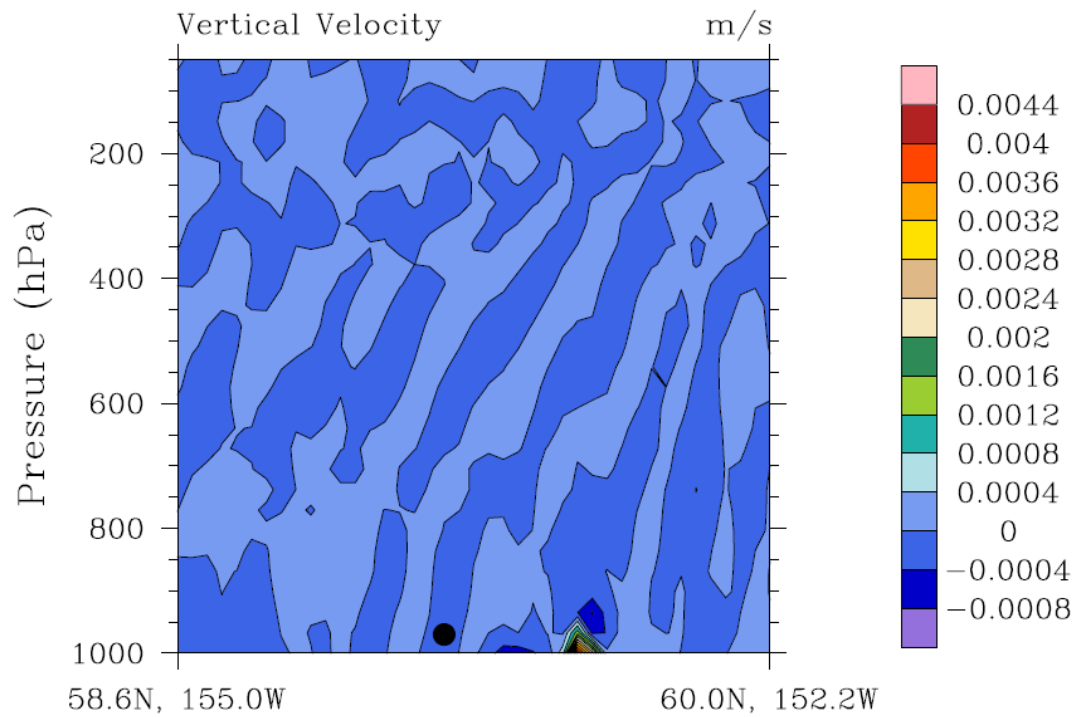


Figure 4.7 Vertical cross-section across domain A, diagonally; the black dot indicates the location of the Augustine on January 25. The vertical velocity is the difference between the water vapor release (hVca) minus the control (hvca) simulations.

ice particles convert to hydrometeors that precipitate out or moisten the atmosphere below the cloud base if evaporation or sublimation occurs.

Coupling water vapor with heat release (HVca) simulation shows an increase in buoyancy and vertical motion at the surface as compared to hvca (Fig. 4.8), resulting in similar effects as the volcanic water vapor release alone (hVca simulation).

Heat release from Augustine (Hvca) significantly increases the near-surface air temperatures downwind of the volcano (Fig. 4.9), as well as vertical motion (Table 4.1) from added buoyancy. Shifts from cloud particles to ice particles as well as the increase in vertical motion lead to an overall significant increase in precipitation.

The ANOVA reveals a significant impact of the hypothetical aerosol release scenario on this day (hvCa) on temperature, precipitation, hydrometeor mixing ratios, and vertical motion; changes are very small (Table 4.1). Local effects of aerosols occur only over Augustine, but significant changes did not spread because the cloud cover was not extensive enough over Augustine.

4.3.3 February 2

February 2 had decreasing cloudiness across the domain as the sea-level pressure rose from a retreating synoptic cyclonic system. Changes in atmospheric variables for February 2 are compared to January 25, because the synoptic situation

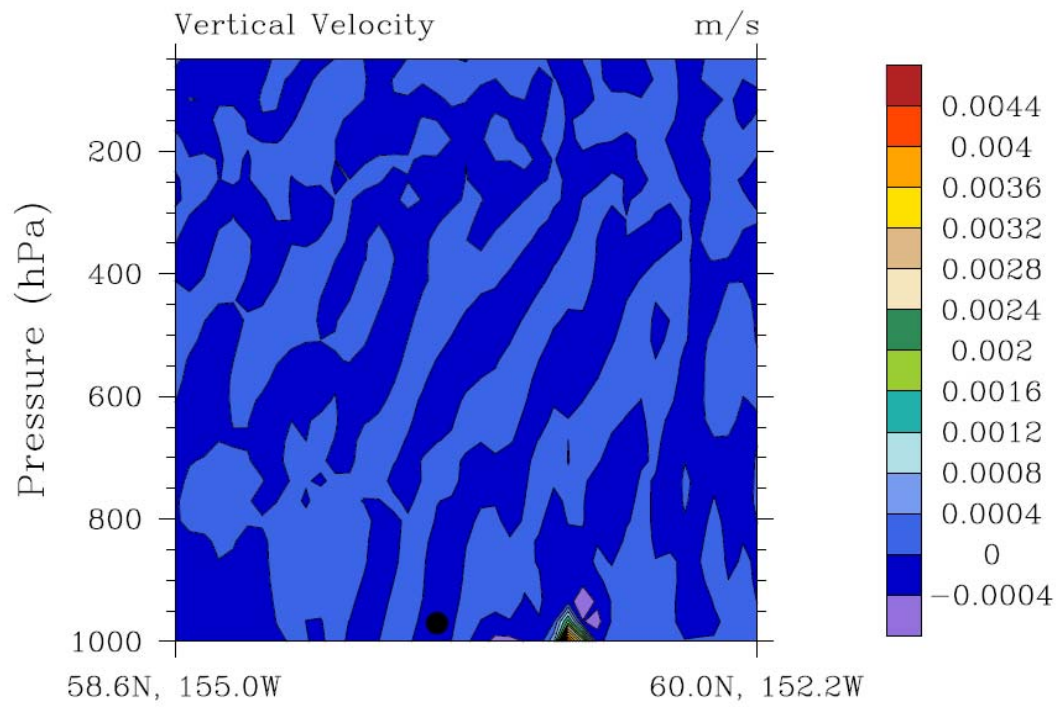


Figure 4.8 Same as 4.6, but for the water vapor and heat release (HVca) simulation.

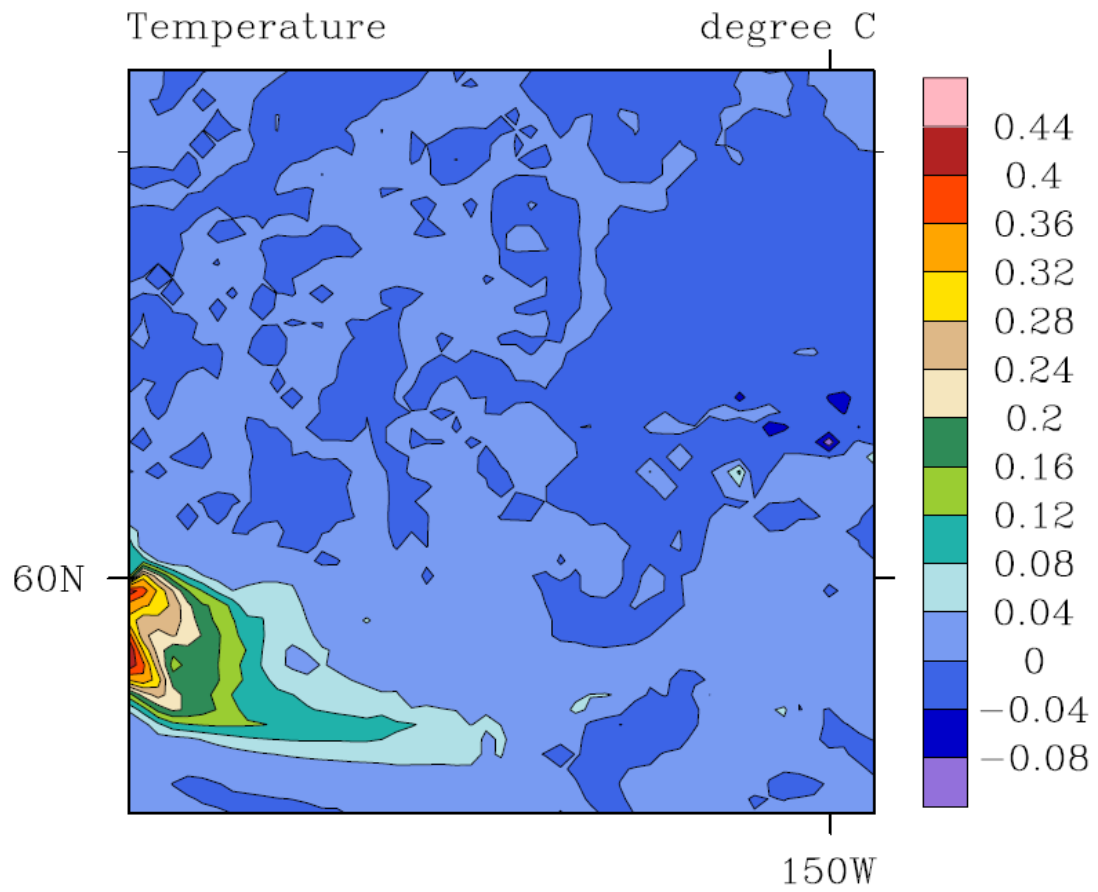


Figure 4.9 Same as 4.6, but for the surface temperature change as a result of the heat release (Hvca) simulation minus the control (hvca) simulation on February 2.

is similar with the exception of February 2 having fewer areas of cloud cover. The notable difference between February 2 and January 25 is that the release of aerosols (hvCa) does not have a significant impact on precipitation (Table 4.7). Since cloud cover is sparse (especially over Augustine itself), significant changes in hydrometeor mixing ratios are very small (a total of 0.02 g/kg for the entire day; Table 4.3).

Volcanic water vapor (hVca) has significant impact on temperature (Fig. 4.10) and precipitation (Fig. 4.11), with higher biases (as much as 21 K and 0.3 mm/h, respectively) as compared with hvca, than on January 25. Vertical velocity and hydrometeor mixing ratios increase by a total of 0.030m/s, and 0.001g/kg, respectively. Lift leads to adiabatic cooling, allowing the atmosphere to achieve supersaturation if sufficient moisture is available (Pruppacher and Klett 1997). More water vapor allows for hydrometeors larger through condensation/deposition, hence precipitation increases. Vertical profiles of cloud ice mixing ratio and vertical velocity are equivalent in structure as the cases on January 25 (Figs. 4.7 and 4.8).

The volcanic release of heat (Hvca) leads to a decrease in precipitation by a total of 14mm/h for the entire day, which indicates that the increase in air-temperatures yields higher saturation mixing ratios for which less condensation/deposition of excess water vapor occurs compared to hvca. Adding heat leads to an increase in vapor pressure required for cloud particles to form (Table 4.2). Vertical profiles of cloud ice mixing ratio and vertical velocity are equivalent in structure as the cases on January 25 (Figs. 4.7 and 4.8).

Table 4.7 Same as 4.5 but for February 2, 2006.

Simulation	MS	F value
hvcA	4.0×10^{-14}	7.9×10^{-11}
hVca	7.2×10^{-06}	0.001
Hvca	1.4×10^{-05}	0.0008
hVca	7.9×10^{-07}	5.9×10^{-05}
hVca	7.9×10^{-07}	5.9×10^{-05}
HvCa	1.7×10^{-07}	0.0001
hVCA	1.7×10^{-07}	0.0001
HVca	8.3×10^{-06}	0.0002
hVcA	4.0×10^{-14}	7.9×10^{-11}
HvcA	1.7×10^{-07}	7.9×10^{-11}
HVCa	4.0×10^{-14}	0.0001
HVcA	4.0×10^{-14}	7.9×10^{-11}
HvCA	4.0×10^{-14}	7.9×10^{-11}
hVCA	4.0×10^{-14}	7.9×10^{-11}
HVCA	4.0×10^{-14}	7.9×10^{-11}

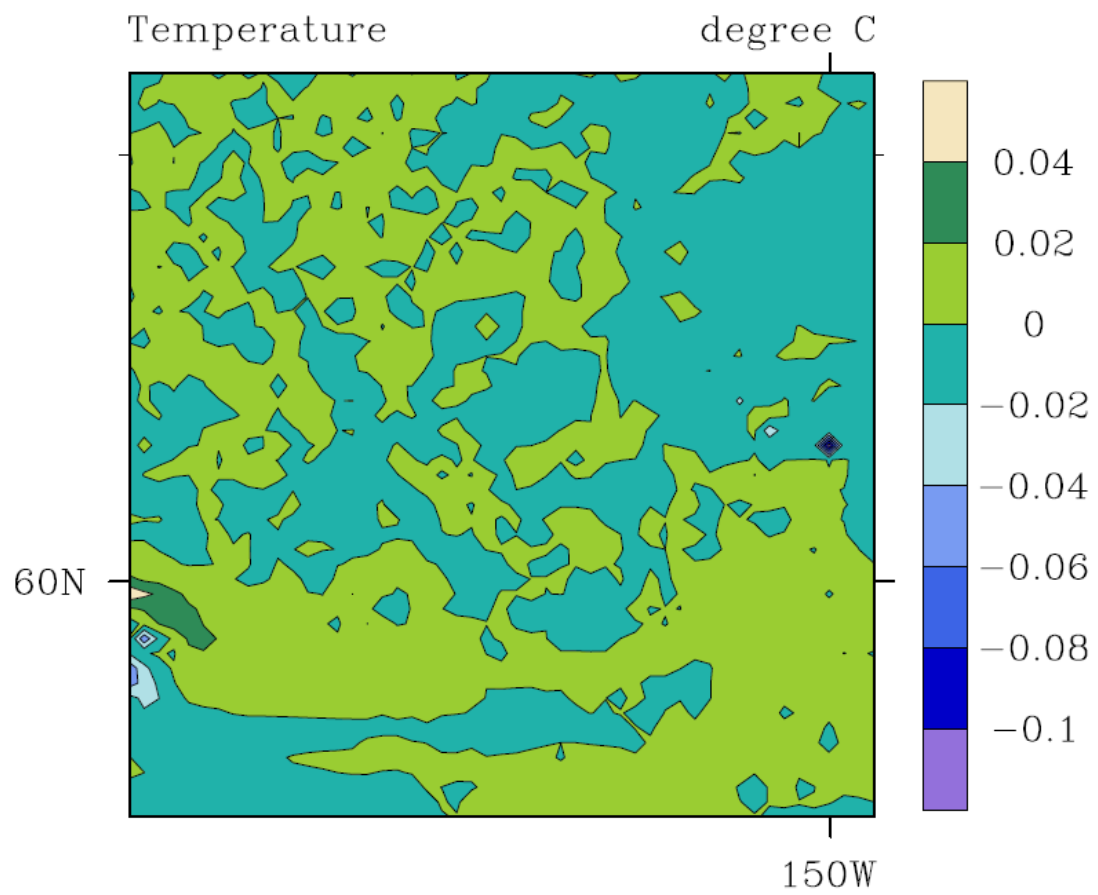


Figure 4.10 Difference between the water vapor release (hVca) and control (hvca) simulation for temperature on February 2.

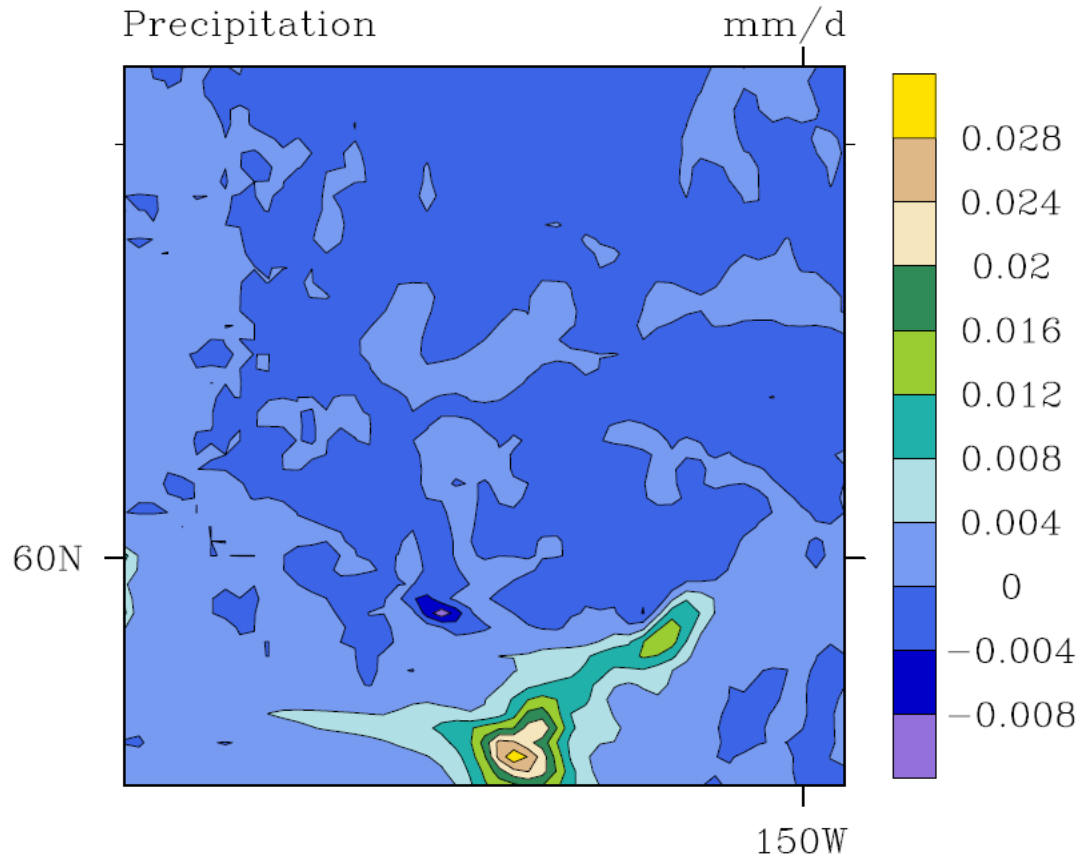


Figure 4.11 Difference between the water vapor release (hVca) and control (hvca) simulation for precipitation on February 2.

Concurrent release of water vapor and heat (HVca) amplifies the eruption effect on precipitation, increasing precipitation by a total of 0.4mm/h. Surface heating leads to buoyant energy and lift, which is important for precipitation formation. Vertical profiles of cloud ice mixing ratio and vertical velocity are equivalent in structure as the cases on January 25 (Fig. 4.8).

Concurrent release of heat and aerosols (HvCa) leads to more precipitation (as much as 0.05 mm/h; Fig. 4.12). In the HvCa case, surface heating leads to vertical motion (Fig. 4.13), thus precipitation increases with vertical lift if enough water vapor is present.

4.3.4 January 30

On January 30, Augustine was in the middle of its continuous phase. Precipitation and cloudiness across the domain was scattered, meaning only a few locations experienced precipitation on this day. Areas downwind of the volcano were generally dry; however, the wind direction in the lower ABL is towards the southeast, which is generally open ocean with exception of Kodiak Island. Low-level cloud cover surrounded Augustine Island on this day, which the plume of aerosols, water vapor, and ash was ejected above and traveled south, away from the cloudy areas. Since the ash plume traveled away from the mainland towards the ocean, Kodiak received most of the ash fall (Fig. 2.4), however most ash fell in the ocean because of the prevailing wind direction. This means that the actual area with

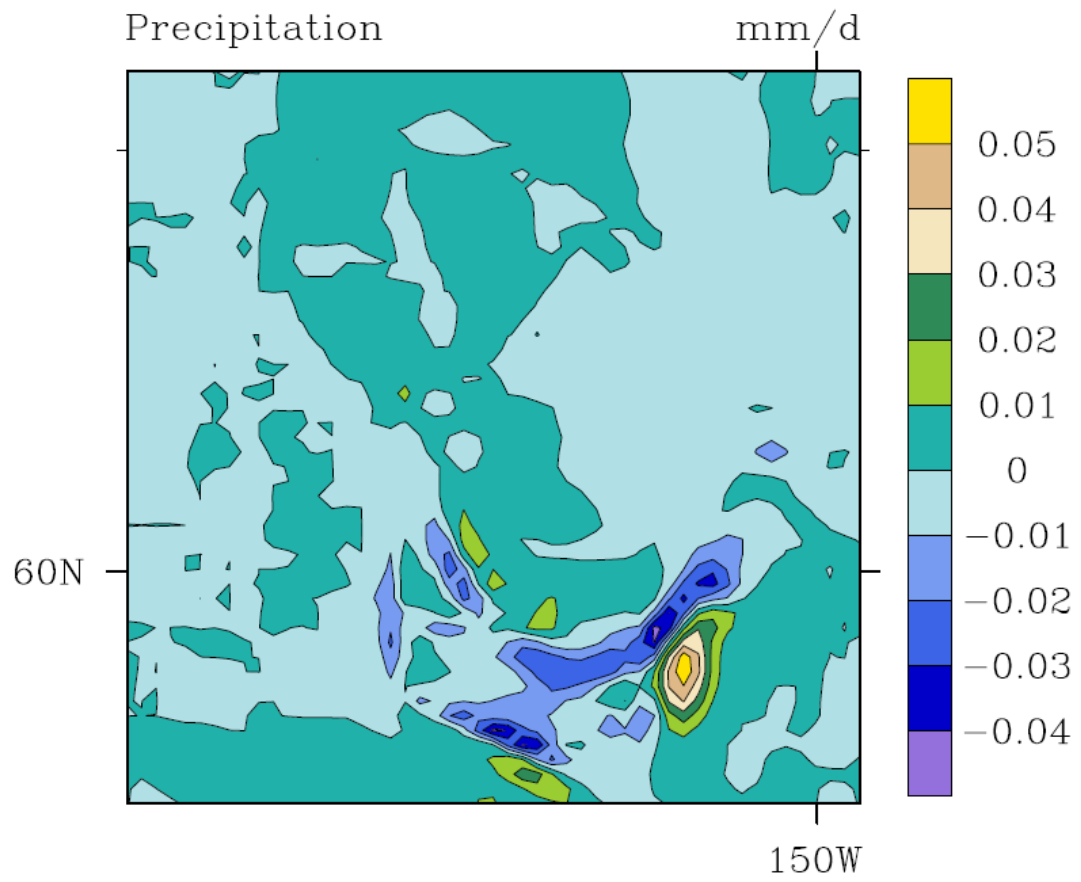


Figure 4.12 Same as 4.10 but for the heat and aerosol release (HvCa) simulation.

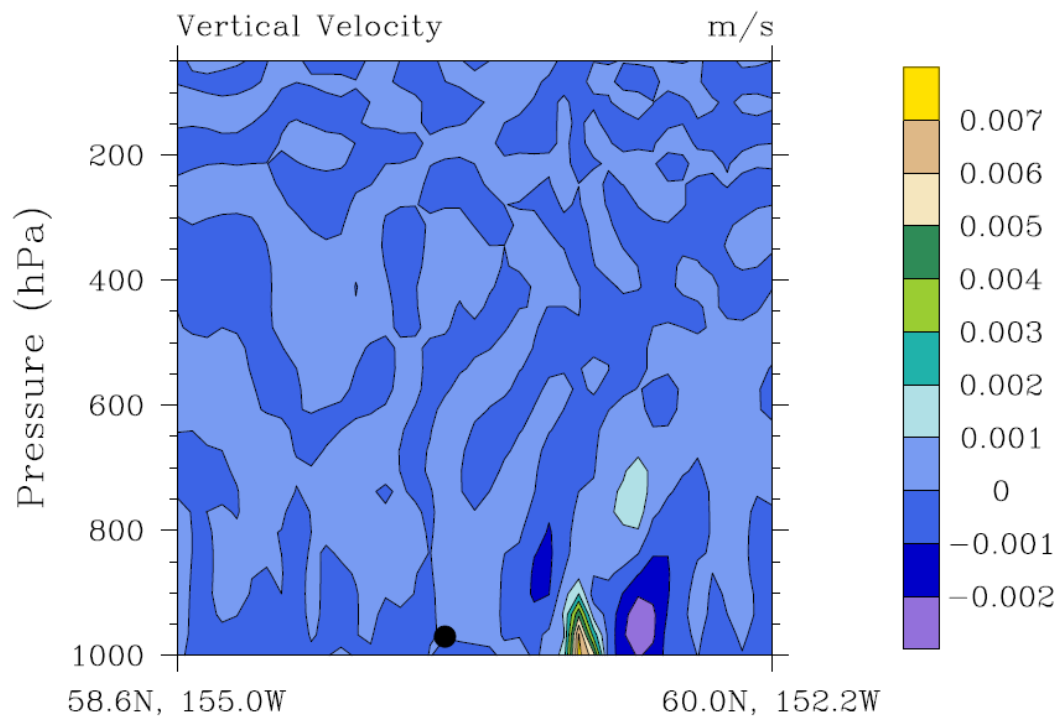


Figure 4.13 Same as 4.6 but for the heat and aerosol release simulation (HvCa) on February 2.

reduced albedo in response to ash fall is small, hence ash fall does not have a significant impact on the weather (Table 4.8).

Volcanic water vapor release has little impact on local weather on January 30, which is one of the few days this occurs. The low-level wind direction is different on January 30 than it is for February 2 and January 25, which likely plays a role in the lack of significant water vapor impact on the weather because the area southeast of Augustine is relatively dry and there is no cloud cover, water vapor could not condense into cloud drops as the plume traveled downwind because the atmosphere is sub-saturated. Due to the relatively dry atmospheric conditions volcanic release of aerosols has very little impact on the weather within the model domain on this day because there is not enough water vapor to reach saturation and make an impact on cloud and precipitation formation.

Heat release (H_{vca}) is significant for surface air-temperature, precipitation, hydrometeor mixing ratios, and vertical velocity in domain A. Precipitation, water vapor mixing ratio, and cloud water mixing ratio decreased by a total of 0.09mm/h (Fig. 4.14), 0.00014kg/kg, and 0.00013kg/kg respectively for domain B (Table 4.4). As pointed out before, heat release is considered in the surface energy balance by an increase of surface temperature as described in the hypothetical scenario (Fig. 2.3). Thus, the vertical temperature profile changed through vertical (Fig. 4.15) and horizontal transport, for which the cloud cover that existed around the island decreases because higher temperatures require a higher water vapor pressure to reach

Table 4.8 Same as 4.5 but for January 30, 2006.

Simulation	MS	F value
hvcA	4.7×10^{-11}	2.2×10^{-08}
hVca	1.3×10^{-09}	3.6×10^{-07}
Hvca	6.5×10^{-09}	7.3×10^{-06}
hVca	1.0×10^{-09}	1.7×10^{-07}
hVca	8.5×10^{-10}	1.2×10^{-07}
HvCa	1.5×10^{-09}	2.8×10^{-07}
hVCA	1.0×10^{-09}	2.0×10^{-07}
HVca	1.3×10^{-09}	5.9×10^{-07}
hVcA	4.7×10^{-11}	2.2×10^{-08}
HvcA	4.7×10^{-11}	2.2×10^{-08}
HVCa	1.0×10^{-09}	2.0×10^{-07}
HVcA	4.7×10^{-11}	2.22×10^{-08}
HvCA	4.7×10^{-11}	2.21×10^{-08}
hVCA	4.7×10^{-11}	2.2×10^{-08}
HVCA	4.7×10^{-11}	2.2×10^{-08}

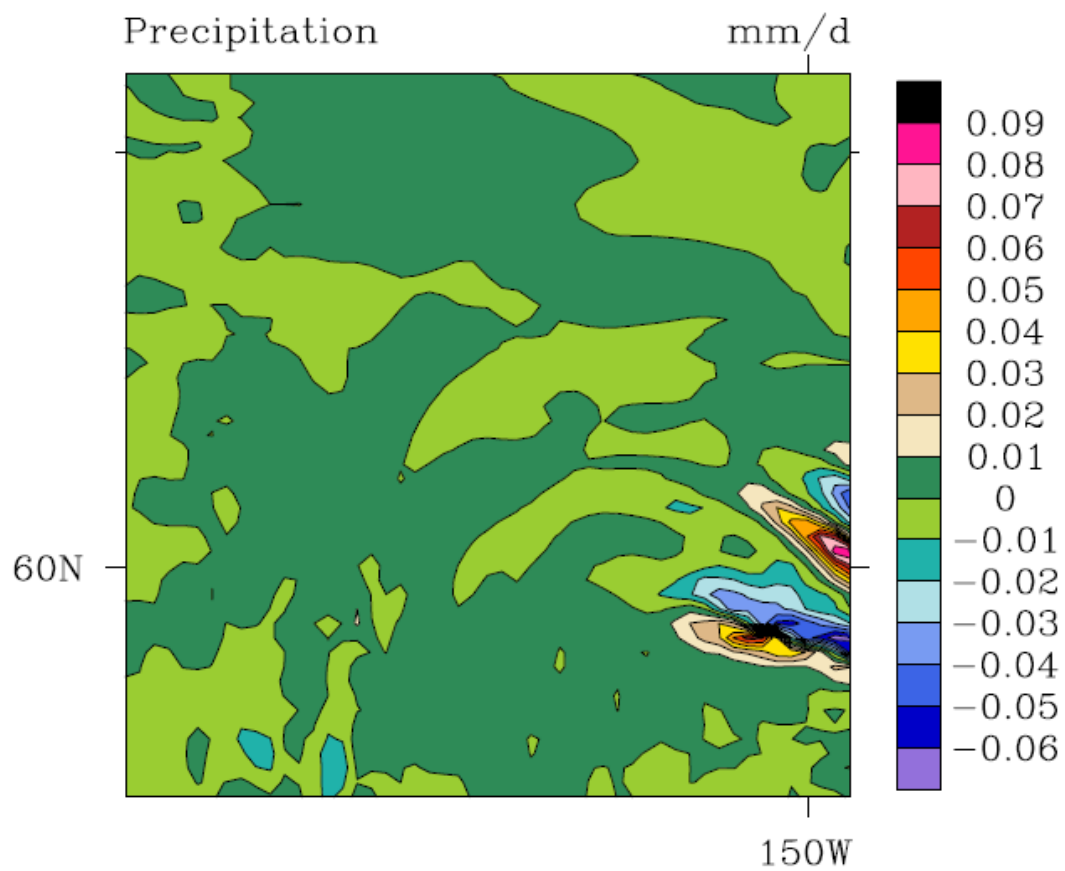


Figure 4.14 Same as 4.10 but for the heat simulation (Hvca) on January 30.

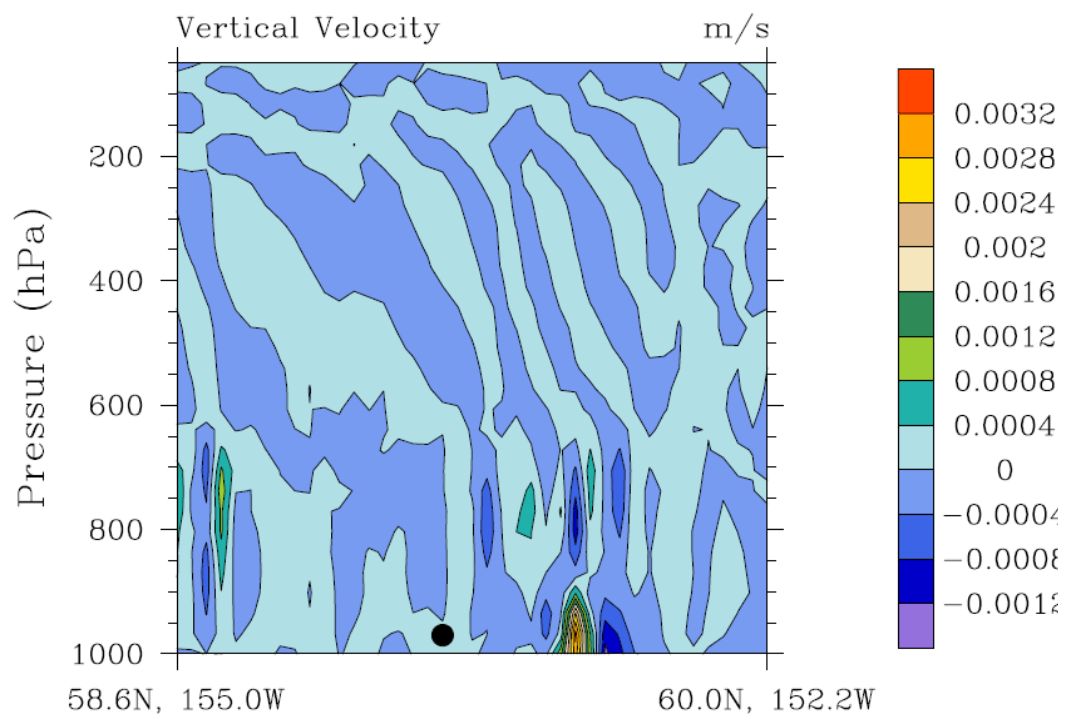


Figure 4.15 Same as 4.6 but for the heat release simulation (Hvca) on January 30.

saturation. Note in the vertical velocity, a wave pattern is formed. Upward motion leads to divergence aloft and convergence at the surface. Due to conservation of mass, downward motion must occur to compensate for the upward motion, which is clearly seen in Fig. 4.15.

Interaction effects of heat and aerosols (HvCa), aerosols and ash fall (hvCA), heat and water vapor (HVca), and heat, water vapor, and ash fall (HvcA) have a significant impact on all of domain B for both temperature and precipitation. The mechanisms that lead to these interactions follow the same mechanisms the individual effects do, which were discussed earlier.

Concurrent release of water vapor and aerosols (hVcA) has no significant impact on temperature, but it increases precipitation by a total of 49.1mm/h domain B (Table 4.4). The mechanism is similar to that discussed earlier; however the changes are close in proximity to the volcano. The aerosols in the plume provide surface area for solid and liquid cloud particles to form on; the water vapor allows the atmosphere to reach saturation. Therefore, the available water vapor is able to produce more hydrometeors and, hence, increase precipitation (Table 4.4).

The secondary interaction of HVcA shows significant impacts on temperature, precipitation, and microphysics for the domain downwind of Augustine. According to the ash fall vector scenarios discussed in chapter 2 (Fig 2.4), ash was able to stay aloft long enough to eventually deposit in areas northeast of Augustine, leading to a decrease in surface albedo. The temperature-albedo feedback results in

an increase in surface temperature, which enhances vertical motion and aids in the formation of clouds because air parcels reach higher levels and become saturated. The combination of ash fall, water vapor, and heat (HvcA) is able to impact the atmosphere by increasing surface air-temperature and precipitation. The warmer surface temperature due to the temperature-albedo feedback increases vertical velocity (Table 4.4) and additional available water vapor increases the cloud water and cloud ice mixing ratios; an increase in water vapor with no increase in available CCN means an increase in cloud and ice particle radii. As discussed earlier, this leads to an increase in precipitation.

4.3.5 January 29

On January 29, Augustine had just switched from its eruptive phase to its continuous phase. Areas nearby the volcano and to the southwest had precipitation, however most of the area was relatively clear and dry.

Domain A precipitation is only significantly impacted by the release of water vapor (hVca), the release of aerosols with concurrent ash fall (hvCA), and the concurrent release of heat, water vapor and aerosols (HVCa). However, significant impact on hydrometeor mixing ratio and vertical velocity is found for simulations of 1) water vapor release (hVca), 2) heat release (Hvca), 3) aerosol release (hvCa), 4) water vapor and aerosol release (hVCA), 5) heat and aerosol release (HvCa), 6) aerosol release and ash fall (hvCA), and 7) water vapor and heat release (HVca). The

impact is documented by changes in cloud cover, which indirectly impacted surface temperature via the processes explained earlier (Table 4.5).

Generally, volcano influences lead to a decrease in ice particle mixing ratios and vertical velocity on this day (Table 4.5 and Figs. 4.16 and 4.17). Changes in temperature and precipitation are small, which means changes in regional weather are subtle. As pointed out above, January 29 was a dry, stable day and Augustine was in its continuous phase, yet atmospheric variables are not significantly impacted by the assumed volcanic factors because the synoptic situation was not favorable for cloud and precipitation processes. This finding in conjunction to the cases discussed in section 4.3.4, 4.3.3, and 4.3.2 indicate that synoptic situations with clouds and precipitation are more sensitive to volcanic eruptions in the continuous phase.

4.4 Summary of Augustine Effects

The various volcanic effects (and combinations of effects) of the 2006 Augustine volcano eruption have the greatest significant impact on daily, regional weather during the continuous phase of the eruption. January 25 and February 2 had widespread precipitation and cloud cover, which likely favored the significant change in atmospheric variables on those days.

Most days examined experienced significant changes for hVca, Hvca, hvCa, hVCa, HvCa, hvCA, and HVca. Temperature generally increases significantly across the domain downwind of Augustine. Reasons for the significant increase in

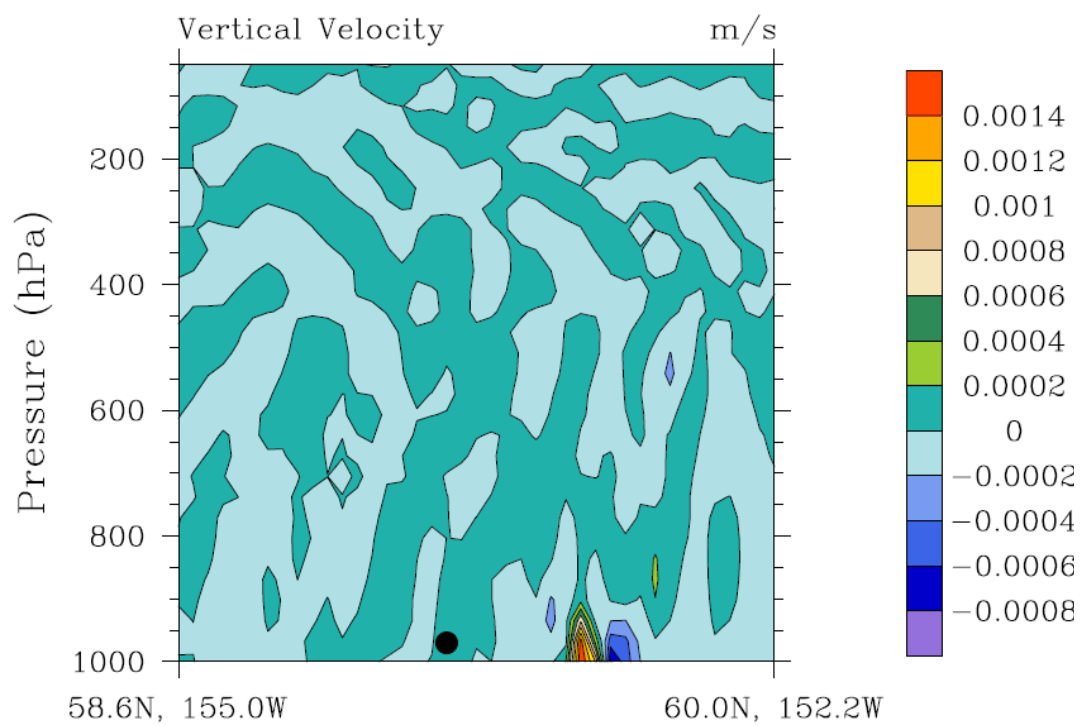


Figure 4.16 Same as 4.6 but for the heat release simulation (Hvca) on January 29.

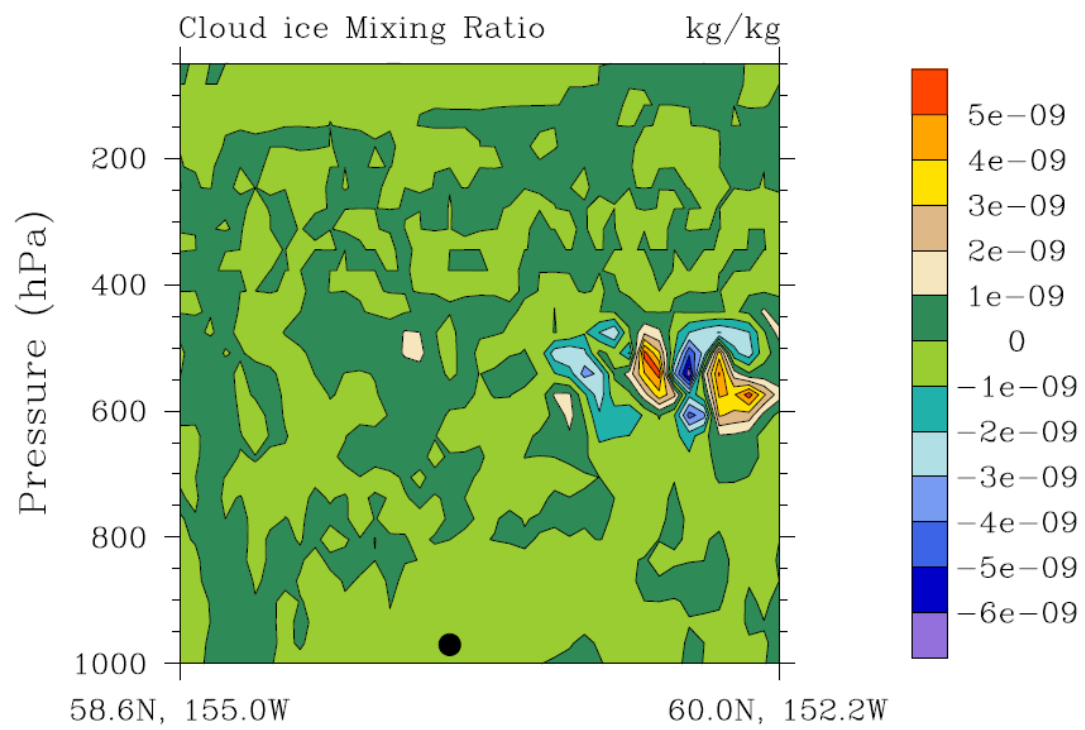


Figure 4.17 Same as 4.6 but for cloud ice mixing ratio for heat release (Hvca) on January 30.

temperature are (1) energy in the form of heat released from Augustine during an eruption period, (2) increased cloud cover due to water vapor release, and (3) the interaction between heat release and water vapor release.

These results from volcanic water vapor, heat, and aerosol release are consistent with those found for water vapor, heat and aerosol release from anthropogenic sources found by Mölders and Olson (2004). They found that anthropogenic releases of aerosols and moisture statistically significantly affect downwind precipitation with 95% confidence; the significant response to aerosol release results from changes in cloud microphysical processes (i.e., changes in cloud to ice particle ratios).

Precipitation generally decreases for the domain downwind of Augustine. Reasons for significant decrease in precipitation are (1) aerosol release leads to smaller, more numerous cloud and ice particles, (2) heat release exponentially increased the amount of water vapor required for saturation and precipitation formation, (3) the interaction between aerosol and heat amplified this result. Water vapor release significantly increases precipitation because it provides moisture needed for saturation and formation of precipitation; heat sometimes increases precipitation because it increases vertical velocity from near-surface heating, thus, air reaches higher levels where they cool enough to reach saturation and the ice phase becomes the dominant precipitation process. The interaction between water vapor and aerosol release significantly increases precipitation as well, because the

extra water vapor allows for cloud particles to grow large enough for precipitation to occur.

5. Conclusions

The Weather Research and Forecasting (WRF) mesoscale model is used to determine the impact of the Augustine Volcanic eruption on local/regional, daily weather. Volcanic eruptions release, among other things, water vapor, heat, CCN/IN, and ash into the atmosphere; ash particles deposit out of the atmosphere quickly, leaving a dark layer of ash over the snow-covered surface.

To determine the impact of these four volcanic influences on local weather, 16 simulations are run using the WRF model. The first simulation serves as a control run, where no volcanic factors are considered. The next four runs include individual consideration of heat release, water vapor release, CCN/IN sized aerosol release, and ash fall. The other 11 simulations include all possible primary, secondary, and tertiary interactions between the four volcanic factors. Data for the Augustine heat released is derived from the NOAA Advanced High Resolution Radiometer (AVHRR; data provided by Dehn, Alaska Volcano Observatory, 2006). Maximum and minimum values of CCN/IN and water vapor release (determined from previous arctic volcanic eruptions) are interpolated to fit the heat release trend for simplicity of the experimental design. Ash fall is considered only on days when ash fall was observed, based on reports provided by Wallace and the Alaska Volcano Observatory (2006).

To analyze the significance of the volcanic influences on daily weather, Analysis of Variance (ANOVA) is used. The ANOVA design works using a null hypothesis;

in this case, the **null hypothesis** is that *the Augustine volcanic eruption had no impact on local/regional, daily weather.*

The simulation without volcanic effects is evaluated by observations from 17 sites with hourly reported data and 26 sites with daily reported data. Overall, WRF showed very good performance when skill is compared with previous model evaluation studies of WRF and other mesoscale models. Though it may not always simulate the values correctly, it captures the trends extremely well (i.e., precisely). In general, WRF tends to overestimate dew-point temperature, wind speed, precipitation, and air temperature; and generally underestimates sea-level pressure and cloud presence for the episode considered here. The results of the model evaluation indicate that WRF can be used to reliably examine the effects of four factors of the Augustine volcanic eruption on local, regional weather.

The ANOVA showed that the examined aspects of the Augustine eruption have the largest statistically significant (at 95% or higher confidence level) impact on daily, regional weather during the continuous phase of the eruption for this hypothetical scenario. However, changes in cloud microphysical processes and cloud and hydrometeor mixing ratios and near-surface variables are most significant when the synoptic situation is favorable for cloud cover and precipitation formation. Most of the days at the end of the period had widespread precipitation and cloud cover.

Most days during the eruption period experienced significant changes for the water vapor, heat, and aerosols simulations, as well as the interactions between water vapor and aerosols (hVCa), heat and aerosols (HvCa), ash fall and aerosols (hvCA), and heat and water vapor simulations (HVca). Temperature generally increases significantly across the domain downwind of Augustine for water vapor, heat, aerosol, and the combined effects from aerosols and ash fall. However, when aerosol effects are considered on days with little to no cloud existence, any simulation that includes the aerosol release tends to not be significant. Precipitation generally decreased (by as much as 0.02mm/d, or 0.1%) for the domain downwind of Augustine for the aerosol simulation (hvCa), precipitation increased for the downwind domain by as much as 0.02mm/h for the water vapor (hVca) and, occasionally, heat (Hvca) simulations. Simulations that consider aerosol release interacting with water vapor (hVCa) or heat (HvCa) generally has significant precipitation increase.

The results of this study add new knowledge on previous studies on volcanic eruptions and their impact on the atmosphere. The short term warming found on a climate scale in response to large volcanic eruptions is seen on a regional scale as well for small volcanic eruptions. The additional heat introduced by the volcano increases buoyant energy. Water vapor from the volcano either leads to a decrease in surface temperature because downward radiation decreases, or warming due to

condensation. The direction of the effect of water vapor depends on the synoptic situation and the amount of water vapor already available in the atmosphere.

Generally, the additional CCNs and INs decrease hydrometeor radii by increasing the number concentration of liquid and solid cloud particles. Consequently, the transformation of cloud particles to hydrometeors by collection slows down which significantly lowers precipitation overall up to 0.04 mm/h, or 0.1%. This process is more likely to occur on days where there is widespread precipitation or heavy, short precipitation events.

Future studies should evaluate the impacts on regional and local weather on a continuous time line. Ash fall may have had a more significant impact if considered over a period longer than a day. Effects from volcanic eruptions can “linger” in the atmosphere, especially over periods of synoptic stability and high-pressure systems. Hence, volcanic effects may extend beyond the day of the eruption and cause a delay of impact in atmospheric variables, particularly for areas far downwind of the volcano. However, such investigations would require high resolved global models that can capture longer time scales than mesoscale models like WRF. As of today high resolved GCMs with a similar resolution like used in this study do not exist for which such investigations have to be postponed to the future.

Further investigation of the aerosols impact on the atmosphere can be done using WRFchem (Grell et al. 2005). Not only does WRFchem allow for the transport of aerosols in the atmosphere, it considers radiative effects of the aerosol layer based

on concentration. The most common CCN released from volcanic eruptions is SO_4^{2-} , which forms from the chemical reaction of available water vapor in the atmosphere and sulfur dioxide (SO_2) from volcanic eruptions. If enough water vapor is available in the atmosphere, conditions are favorable for these chemical reactions to take place; thus cloud hydrometeors formed from microphysical processes are more acidic. To investigate the impact of the volcanic SO_2 release on the acidity of precipitation for the surrounding area, the WRFchem can be used. WRFchem consists of the WRF model coupled with an online chemistry package.

As measurements of aerosol concentration, water vapor concentration, and ash plume dispersion become available, more realistic scenarios based on the Augustine eruption can be validated using various models. With this research, the basic microphysical processes are known. In future research, small-scale models considering more complex atmospheric processes can be used to further the understanding of dynamic and physical processes of the eruption impact on local, mesoscale weather.

REFERENCES

- Anthes, R.A., 1983: Regional models of the atmosphere in middle latitudes. *Mon. Wea. Rev.*, **111**, 1306-1335.
- Anthes, R.A., Y.H. Kuo, E.Y. Hsie, S. Low-Nam, and T.W. Bettge, 1989: Estimation of skill and uncertainty in regional numerical models. *Quart. J. Roy. Meteorol. Soc.*, **111**, 763-806.
- Avissar, R. and R.A. Pielke, 1989: A parameterization of heterogeneous land surface for atmospheric numerical models and its impact on regional meteorology. *Mon. Wea. Rev.*, **117**, 2113-2136.
- AVO, cited 2007: Augustine description and statistics. [Available online at <http://www.avo.alaska.edu/volcanoes/volcinfo.php?volcname=Augustine>].
- Berry, E.X. and R.L. Reinhardt 1974: An analysis of cloud drop growth by collection. Part II: Single initial distributions. *J. Atmos. Sci.*, **31**, 2127-2135.
- Boone, A., F. Habets, J. Noilhan, D. Clark, P. Dirmeyer, Y. Gusev, O. Nasonova, I. Haddeland, R. Koster, D. Lohmann, K. Mitchell, G.-Y. Niu, S. Fox, A. Pitman, J. Polcher, S. V erant, A.B. Shmakin, K. Tanaka, B. van den Hurk, D. Verseghy, P. Viterbo, S. Mahanama, and Z.-L. Yang, 2004: The Rh one-aggregation Land Surface Scheme intercomparison project: An overview. *J. Geophys. Res.*, **97**, 7603-7612.
- Caires S, V.R. Swail, and X.L. Wang, 2006: Projection and analysis of extreme wave climate. *J. Climate*, **19**, 5581–5605.
- Cheng, W.Y.Y. and W.J. Steenburgh, 2005: Evaluation of surface sensible weather forecasts by the WRF and the Eta models over the western United States. *Wea. Forecast.*, **20**, 812-821.
- Colle B. A., C. F. Mass, and D. Ovens, 2001: Evaluation of the timing and strength of MM5 and Eta surface trough passages over the Eastern Pacific. *Wea Forecasting*, **16**, 553-572.
- Collins, R.L., J. Fochesatto, K. Sassen, P.W. Webley, D.E. Atkinson, K.G. Dean, C.F. Cahill, and M. Kohei, 2007: Predicting and validating the motion of an ash cloud during the 2006 eruption of Mount Augustine volcano, Alaska, USA. *J. Nat. Inst. Infor. Comm. Tech.*, **54**, 17-28.

- Cooper, W.A., 1986: Ice initiation in natural clouds. Precipitation enhancement- A scientific challenge. *Meteor. Monogr.*, **43**, Amer. Met. Soc., 29-32.
- Davis, C.A., B. Brown, and R. Bullock, 2006: Object-based verification of precipitation forecasts. Part I: Methodology and application to mesoscale rain areas. *Mon. Wea. Rev.*, **134**, 1772-1784.
- Dingman, S. L., 1994: *Physical Hydrology*, Macmillan Publishing Company, 575 pp.
- Done, J., C.A. Davis, and M. Weisman, 2004: The next generation of NWP: explicit forecasts of convection using the weather research and forecasting (WRF) model. *Atmos. Sci. Lett.*, **5**, 110-117.
- Dudhia, J., 1989: Numerical study of convection observed during the winter monsoon experiment using a mesoscale two-dimensional model, *J. Atmos. Sci.*, **46**, 3077-3107.
- Fröhlich, K. and N. Mölders, 2002: Investigations on the impact of explicitly predicted snow metamorphism on the microclimate simulated by a meso-beta/gamma-scale non-hydrostatic model. *Atmos. Res.*, **62**, 71-109.
- Grell, G. A., J. Dudhia, and D. R. Stauffer, 1995: A description of the fifth generation Penn State/NCAR mesoscale model (MM5). NCAR Tech Note NCAR/TN-398+STR, 138 pp. [Available from NCAR Publications Office, P. O. Box 3000, Boulder, CO 80307-3000.].
- Grell, G.A. and D. Devenyi, 2002: A generalized approach to parameterizing convection combining ensemble and data assimilation techniques. *Geophys. Res. Lett.*, **29**(14), Article 1693.
- Grell, G. A., S. E. Peckham, R. Schmitz, S. A. McKeen, G. Frost, W. C. Skamarock, and B. Eder, 2005: Fully coupled “online” chemistry within the WRF model. *Atmos. Environ.*, **39**(37), 6957-6975.
- Gyakum J. R., M. Carrera , D.-L. Zhang, S. Miller, J. Caveen, R. Benoit, J. Mailhot, T. Black, A. Buzzi, M. Fantini, C. Folloni, P. Malguzzi, C. Chouinard, J. J. Katzfey, J. L. McGregor, Y.-H. Kuo, S. Low-Nam, F. Lalaurette, M. Nakamura, G. Tripoli, and C. Wilson, 1996: A Regional Model Intercomparison Using a Case of Explosive Oceanic Cyclogenesis. *Wea. Forecasting*, **11**, 521-543.

- Hart K. A., W. J. Steenburgh, D. J. Onton, and A. J. Siffert, 2003: An evaluation of mesoscale model based model output statistics (MOS) during the 2002 Olympic and Paralympic Winter Games. *Wea. Forecasting*, **19**, 200-218.
- Henderson, D., D. PaiMazumder, and N. Mölders, cited 2007: Comparison of Weather Research and Forecasting (WRF) model simulations with NCEP reanalysis data over Siberia. [http://www.gi.alaska.edu/~molders/REU_report_2007.pdf].
- Hines K. M. and D. H. Bromwich, 2008: Development and testing of Polar Weather Research and Forecasting (WRF) Model. Part I: Greenland Ice Sheet meteorology. *Mon. Wea. Rev.*, **136**, 1971-1989.
- Hobbs, P.V., J.P. Tuell, D.A. Hegg, L.F. Radke, and M.W. Eltgroth, 1982: Particles and gases in the emissions from the 1980-1981 volcanic eruptions of Mt. St. Helens. *J. Geophys. Res.*, **87**, 11062-11086.
- Hobbs, P.V., L.F. Radke, J.H. Lyons, R.J. Ferek, D.J. Coffman, and T.J. Casadevall, 1991: Airborne measurements of particle and gas emissions from the 1990 volcanic eruptions of Mount Redoubt. *J. Geophys. Res.*, **96**, 18,735-18,752.
- Hong, S.-Y. and H.-L. Pan, 1996: Nonlocal boundary layer vertical diffusion in a medium-range forecast model, *Mon. Wea. Rev.*, **124**, 2322-2339.
- Houghton, J.T., G.J. Jenkins, and J.J. Ephraums, 1990: *Climate change: The IPCC scientific assessment*. Cambridge University Press, 365 pp.
- Jacob, D.J., 1999: *Introduction to Atmospheric Chemistry*. Princeton University Press, 264 pp.
- Kirchner, I., G.L. Stenchikov, H.-F. Graf, A. Robock, and J.C. Antuña, 1999: Climate model simulation of winter warming and summer cooling following the 1991 Mount Pinatubo volcanic eruption. *J. Geophys. Res.*, **104D**, 19039-19056.
- Kramm, G., R. Dlugi, G.J. Dollard, T. Foken, N. Mölders, H. Müller, W. Seiler, and H. Sievering, 1995: On the dry deposition of ozone and reactive nitrogen compounds. *Atmos. Environ.*, **29**, 3209-3231.
- Li, Z., U. S. Bhatt, and N. Mölders, 2008: Impact of doubled CO₂ on the interaction between the global and regional water cycles in four study regions. *Climate Dyn.*, **30**, 255-275.

- Mass, C. and A. Robock, 1982: The short-term influence of the Mount St. Helens volcanic eruption on surface temperature in the Northwest United States. *Mon. Wea. Rev.*, **110**, 614-622.
- Mather, T.A., D.M. Pyle, and C. Oppenheimer, 2003: Tropospheric volcanic aerosol. *Volcanism and the Earth's Atmosphere, Geophys.*, **139**, American Geophysical Union, 189-212.
- Mlawer, E.J., S.J. Taubman, P.D. Brown, M.J. Iacono, and S.A. Clough, 1997: Radiativetransfer for inhomogeneous atmosphere: RRTM, a validated correlated-k model for the longwave. *J. Geophys. Res.*, **102** (D14), 16663-16682.
- Mölders, N., 2008: Suitability of the Weather Research and Forecasting (WRF) model to predict the June 2005 fire weather for Interior Alaska. *Wea. Forecast.* (in press).
- Mölders, N., U. Haferkorn, J. Döring, and G. Kramm, 2003: Long-term numerical investigations on the water budget quantities predicted by the hydro-thermodynamic soil vegetation scheme (HTSVS) - Part II: Evaluation, sensitivity, and uncertainty. *Meteor. Atmos. Phys.*, **84**, 137-156.
- Mölders, N. and M.A. Olson, 2004: Impact of urban effects on precipitation in high latitudes. *J. Hydrometeor.*, **5**, 409-429.
- Mölders, N. and J.E. Walsh, 2004: Atmospheric response to soil-frost and snow in Alaska in March. *Theor. Appl. Climat.*, **77**, 77-105.
- Montgomery, D.C., 1976: *Design and Analysis of Experiments*. 3rd ed. Wiley and Sons, 418 pp.
- Narapusetty, B. and N. Mölders, 2005: Evaluation of snow depth and soil temperatures predicted by the Hydro-Thermodynamic Soil-vegetation scheme coupled with the fifth-generation Pennsylvania State University-NCAR mesoscale model. *J. Appl. Meteor.*, **44**, 1827-1843.
- Newhall, C.G. and S. Self, 1982: The volcanic explosivity index (VEI): An estimate of explosive magnitude for historical volcanism. *J. Geophys. Res.*, **87**, 1231-1238.
- Nutter, P.A. and J. Manobianco, 1999: Evaluation of the 29km-Eta Model. Part I: Objective verification at three selected stations. *Wea. Forecast.*, **14**, 5-17.

- Oman, L., A. Robock, G. Stenchikov, G.A. Schmidt, and R. Ruedy, 2005: Climatic response to high-latitude volcanic eruptions. *J. Geophys. Res.*, **110D**, D13103.
- Otkin J. A. and T. J Greenwald, 2008: Comparison of WRF Model-simulated and MODIS-derived cloud data. *Mon. Wea. Rev.*, **136**, 1957-1970.
- PaiMazumder, D., J. Miller, Z. Li, J.E. Walsh, A. Etringer, J. McCreight, T. Zhang, and N. Mölders, 2007: Evaluation of Community Climate System Model soil temperatures using observations from Russia. *Theor. Appl. Climatol.*, doi10.1007/s00704-007-0350-0.
- Pielke R.A., 2002: *Mesoscale Meteorological Modeling*. 2nd ed. Academic Press, 676 pp.
- Power, J.A., C.J. Nye, M.L. Coombs, R.L. Wessels, P.F. Cervelli, J. Dehn, K.L. Wallace, J.T. Freymueller, and M.P. Doukas, 2006: The reawakening of Alaska's Augustine volcano. *Eos*, **87**, 373-377.
- Pruppacher, H.R. and J.D. Klett, 1997: *Microphysics of clouds and precipitation*. 2nd ed. Kluwer Academic Publishers, 954 pp.
- Robock, A., 1981: A latitudinally dependent volcanic dust veil index, and its effect on climate simulations. *J. Volcanol. Geotherm. Res.*, **11**, 67-80.
- Robock, A., 1996: Stratospheric control of climate. *Science*, **272**, 972-973.
- Robock, A., 2000: Volcanic eruptions and climate. *Rev. Geophys.*, **38**, 191-219.
- Robock, A., 2003: Volcanoes: Role in climate. in *Encyclopedia of Atmospheric Sciences*, J. Holton, J. A. Curry, and J. Pyle, Eds., (Academic Press, London), 10.1006/rwas.2002.0169, 2494-2500.
- Robock, A., cited 2007: Publications by Alan Robock on volcanic eruptions and climate [Available online at http://climate.envsci.rutgers.edu/robock/robock_volpapers.html].
- Robock, A. and J. Mao, 1992: Winter warming from large volcanic eruptions. *Geophys. Res. Lett.*, **12**, 2405-2408.
- Robock, A. and J. Mao, 1995: The volcanic signal in surface temperature observations. *J. Climate*, **8**, 1086-1103.

- Rogers, R.R. and M.K. Yau, 1989: *Short Course in Cloud Physics*. Butterworth-Heinemann, 304 pp.
- Ruddiman, W.F., 2001: *Earth's Climate. Past and Future*. W.H. Freeman, 465 pp.
- Sassen K., J. Zhu, P. Webley, K. Dean, and P. Cobb, 2007: Volcanic ash plume identification using polarization lidar: Augustine eruption, Alaska. *Geophys. Res. Lett.*, **34**, L08803, doi:10.1029/2006GL027237.
- Seth, A., F. Giorgi, and R.E. Dickinson, 1994: Simulating fluxes from heterogeneous land surfaces: Explicit subgrid method employing the Biosphere-Atmosphere transfer Scheme (BATS). *J. Geophys. Res.*, **99**, 18 651-18 667.
- Shulski, M. and G. Wendler, 2007: *The Climate of Alaska*. University of Alaska Press, 216 pp.
- Skamarock, W. C., 2004: Evaluating Mesoscale NWP Models Using Kinetic Energy Spectra. *Mon. Wea., Rev.*, **132**, 3019-3032.
- Skamarock, W.C., J.B. Klemp, J. Dudhia, D.O. Gill, D.M. Barker, W. Wang, and J.G. Powers, 2005: A description of the advanced research WRF version 2. NCAR/TN-468+STR, 88 pp.
- Smirnova, T.G., J.M. Brown, and S.G. Benjamin, 1997: Performance of different soil model configurations in simulating ground surface temperature and surface fluxes. *Mon. Wea. Rev.*, **125**, 1870-1884.
- Smirnova, T.G., J.M. Brown, S.G. Benjamin, and D. Kim, 2000: Parameterization of cold season processes in the MAPS land-surface scheme. *J. Geophys. Res.*, **105** (D3), 4077-4086.
- Soden, B.J., R.T. Wetherald, G.L. Stenchikov, and A. Robock, 2002: Global cooling after the eruption of Mount Pinatubo: A test of climate feedback by water vapor. *Science*, **296**, 727-730.
- Stith, J.L., P.V. Hobbs, and L.F. Radke, 1978: Airborne particle and gas measurements in the emissions from six volcanoes. *J. Geophys. Res.*, **83**, 4009-4017.
- Stoss L. A. and S. L. Mullen, 1995: The dependence of short-range 500-mb height forecasts on the initial flow regime. *Wea. Forecasting*, **10**, 353-368.

- Thompson, G., R.M. Rasmussen, and K. Manning, 2004: Explicit forecasts of winter precipitation using an improved bulk microphysics scheme. Part I: Description and sensitivity analysis. *Mon. Wea. Rev.*, **132**, 519-542.
- von Storch, H. and F.W. Zwiers, 1999: *Statistical Analysis in Climate Research*. Cambridge University Press, 484 pp.
- Wallace, J.M. and P.V. Hobbs, 2006: *Atmospheric Science: An Introductory Survey*. 2nd ed. Academic Press, 483 pp.
- Wang, W., D. Barker, C. Bruy`ere, J. Dudhia, D. Gill, and J. Michalakes, 2004: WRF Version 2 modeling system user's guide. <http://www.mmm.ucar.edu/wrf/users/docs/userguide/>.
- Wigley, T.M.L., C.M. Ammann, B.D. Santer, and S.C.B. Raper, 2005: Effect of climate sensitivity on the response to volcanic forcing. *J. Geophys. Res.*, **110**, D09107, doi:10.1029/2004JD005557.
- Wilks, D., 1995: *Statistical Methods in Atmospheric Sciences: An Introduction*. Academic Press, 467 pp.
- Yang D, B.E. Goodison, J.R. Metcalfe, V.S. Golubev, R. Bates, T. Pangburn, and C.L. Hanson, 1998: Accuracy of NWS 8" standard nonrecording precipitation gauge: Results and application of WMO intercomparison. *J. Atmos. Oceanic Technol.*, **15**, 54-68.
- Zhong, S., H. In, X. Bian, J. Charney, W. Heilman, and B. Potter, 2005: Evaluation of real-time high resolution MM5 predictions over the Great Lakes region. *Wea. Forecast.*, **20**, 63-81.
- Zhong, S. and J. Fast, 2003: An evaluation of the MM5, RAMS, and Meso-Eta models at subkilometer resolution using VTMX field campaign data in the Salt Lake Valley. *Mon. Wea. Rev.*, **131**, 1301-1322.